DEVELOPMENT OF BIOCOMPATIBLE DEXTRAN-OXANORBORNADIENE HYDROGELS

A Thesis
Presented to
The Academic Faculty

by

Jessica Lloyd

In Partial Fulfillment
of the Requirements for the Degree
Master of Science in the
School of Chemistry and Biochemistry

Georgia Institute of Technology
August 2019

DEVELOPMENT OF BIOCOMPATIBLE DEXTRAN-OXANORBORNADIENE HYDROGELS

Approved by:

Dr. M.G. Finn, Advisor
School of Chemistry and Biochemistry
Georgia Institute of Technology

Dr. Will Gutekunst
School of Chemistry and Biochemistry
Georgia Institute of Technology

Dr. Amit Reddi
School of Chemistry and Biochemistry
Georgia Institute of Technology

Date Approved: July 12, 2019

ACKNOWLEDGEMENTS

I am so thankful for all of the guidance and support from so many people. I would like to thank my advisor, Dr. M.G. Finn for helping me along on my research, teaching me how to ask better questions, and inspiring me to be a better scientist.

I would like to thank Daisy Johnson and Dr. Havran for all of their hard work and contributions with the OND hydrogel *in vivo* studies.

Thank you to Dr. Johnna Temenoff for allowing me to join the BioMAT training program. It was by far one of my favorite experiences of grad school. I've learned so much not only from being in the program but also from your mentorship.

Thank you to the Finn lab past and present. Special thanks to EBBers, Dr. Liangjun Zhao, Dr. Soumen Das, Robert Hincapie, Asheley Chapman, and Jeffery Noble for your patience and mentorship. The thought of doing chemical reactions on micrograms of product was terrifying, but you all guided me through it. Thanks to Dr. Soumen Das for taking the time to show me how to make Qβ VLPs. Special thanks to MoSE people Dr. Nick Bruno, Breanne Hamlett, Kirstie Thompson, Lucrezia DePascalis, and Ruyi Yang for all of the laughs and constant support. Thanks to Lu for all of the great food suggestions and for helping me with everything related to instrumentation, you truly are a wizard. Thanks to Ruyi for all of the oranges and encouragement.

I would like to thank the best parents in the world, Lynn and David Lloyd. Your unwavering love and support have gotten me to where I am today. Thank you to the best sister in the world, Rebecca Lloyd, for always being there for me. Lastly, I would like to thank Ziv Arzt for always believing in me. I couldn't have done it without you.

TABLE OF CONTENTS

LIST OF TABLES

LIST OF FIGURES

LIST OF SYMBOLS AND ABBREVIATIONS

AF488	Alexa Fluor 488
BSA	bovine serum albumin
CAR	coxsackie and adenovirus receptor
CAR-/-	coxsackie and adenovirus receptor knockout mice
CuAAC	copper-catalyzed azide-alkyne cycloaddition
DAPI	4′,6-diamidino-2-phenylindole
DCC	N,N'-Dicyclohexylcarbodiimide
DCM	dichloromethane
DETC	dendritic epidermal T cells
DI	deionized
DMF	dimethylformamide
DMSO	dimethyl sulfoxide
DTT	dithiothreitol
EtOAc	ethyl acetate
G’	storage modulus
G’’	loss modulus
HATU	1-[Bis(dimethylamino)methylene]-1*H*-1,2,3-triazolo[4,5-*b*]pyridinium 3-oxid hexafluorophosphate
ICAM-1	intercellular adhesion molecule-1
ICAM-1-/-	intercellular adhesion molecule-1 knockout mice
JAML	junction adhesion molecule like
KC	keratinocyte

mCPBA	meta-chloroperoxybenzoic acid
MeOH	methanol
ME OND	methyl ester oxanorbornadiene
MW	molecular weight
MWCO	molecular weight cut off
OND	oxanorbornadiene
PBS	phosphate buffered saline
PEG-SH	polyethylene glycol-thiol
rDA	retro-Diels-Alder
RFP	red fluorescent protein
TxRed	Texas Red
VEGF	vascular endothelial growth factor
VLP	virus-like-particle
Wt%	weight percent

SUMMARY

Hydrogels have garnered much attention over the past few decades for their ability to deliver therapeutics with spatial and temporal control. However, many of these systems can exhibit burst release and are not easily adjusted to realize different release kinetics. The research reported in this thesis aims to develop tunable degradable hydrogels from oxanorbornadiene linkers, which have been shown to have programmable fragmentation rates that can be tuned over an exceptionally wide range of time. OND hydrogels of different crosslinking compositions were all able to form robust gels in as little as seconds and release of entrained cargo was found to be tunable over 0.5 to 25 days by changing the OND substitution or crosslinking system. Oxanorbornadiene hydrogels were then applied to *in vivo* models seeking to improve healing in chronic wounds where it was found that OND hydrogels were able to deliver therapeutic cargo at the expected preprogrammed rates to improve wound healing. Degradable hydrogels comprised of OND cleavable linkages continue to show great promise as simple drug delivery systems that can be widely useful to applications requiring controlled release over hours or months.

CHAPTER 1. Introduction

1.1 General Introduction of Hydrogels

It is well understood that drug potency does not always correlate with therapeutic efficacy but is rather largely dependent on the delivery system of the drug.[1] Low bioavailability, off-target effects, and immunogenicity are all important obstacles to efficient delivery.[1,2] To address these obstacles, research has focused on the development of controlled release delivery systems such as liposomes, nanoparticles, and hydrogels, which are able to release therapeutics with temporal and spatial control.

Hydrogels are water-swollen polymer networks that are able to hold a three-dimensional shape. Networks can be physically crosslinked by noncovalent interactions or chemically crosslinked by water-tolerant reactions such as Michael addition, CuAAC, thiol-ene, and Diels-Alder.[3] Hydrogel materials are typically biocompatible due to their high-water content as well as their stiffness, which can be tuned to match the physical properties of different structural tissues.[4] Another tunable property of hydrogels is their size, which can be cast anywhere from nanometers to centimeters. Nano or micro gels are small enough to pass through needles and are thus often used for injectable administration.[4] On the other hand, larger hydrogels are often used for transdermal delivery and have been investigated in the treatment of wounds.[5]

One of the first hydrogels for a therapeutic application was reported in 1960 by O. Wichterle and D. Lím and described the polymerization of glycomonomethacrylate to form porous transparent gels for contact lenses.[6] Hydrogel delivery systems were reported by

Nalbandian, Henry, and Wilks in 1972 where they used a surfactant based gel to suspend and deliver bactericidal agents to burn wounds.[7] Over the last few decades advancements in hydrogel delivery systems have centered largely on tuning mechanical and degradation profiles to better control release of cargo.

1.2 Hydrogel Release Mechanisms

In order to better control and extend cargo delivery, hydrogels have been engineered to have different release mechanisms (Figure 1). Mechanisms that are dependent on interactions between the cargo and hydrogel network include electrostatic interactions, hydrophobic associations, and cleavable linkages.[4] Affinity based delivery systems have been used to deliver growth factors such as VEGF from heparin based hydrogels over periods of 5 to 7 days.[8,9] Release mechanisms based on hydrophobic associations, such as cyclodextrin inclusion complexes, have been able to achieve similar release kinetics to affinity based delivery systems.[10-12] While both mechanisms are able to extend delivery of cargo when compared to diffusion mechanisms, they can still exhibit burst release kinetics, which is the uncontrolled release of cargo.

Hydrogels that employ cleavable linkages have been shown to achieve slightly longer release timeframes as well as smaller degrees of burst release.[4] Cleavage by β-elimination is one common release mechanism of tethered drugs that has achieved release profiles over 5 to 20 days depending on the linker.[13]

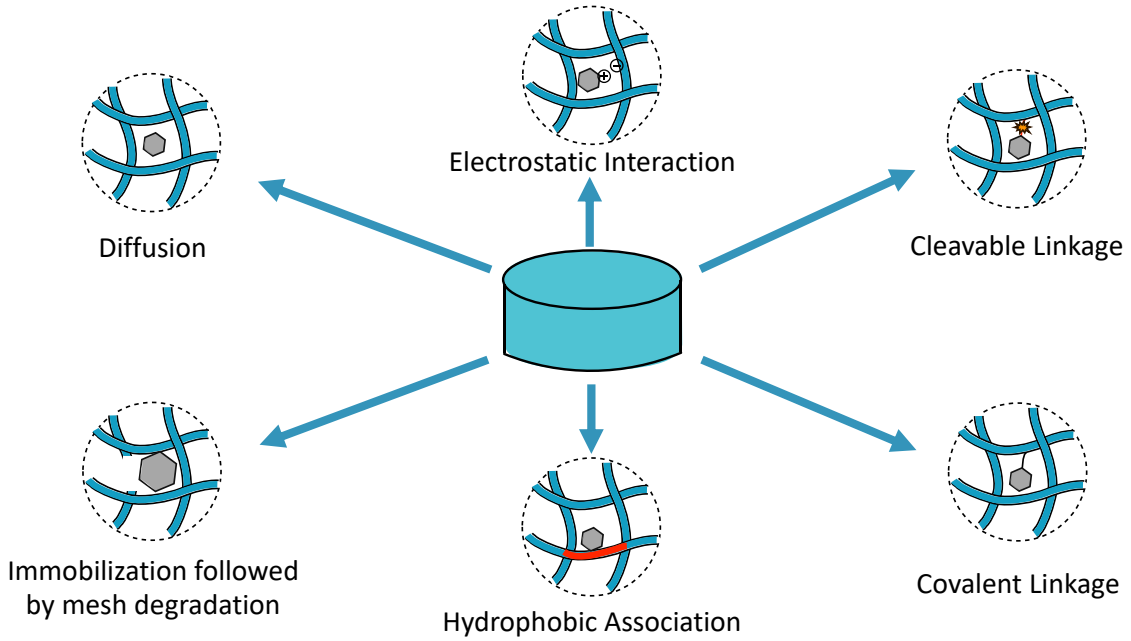

Figure 1. Hydrogel release mechanisms.

Hydrogels are also able to physically entrain (or "trap") drug cargo rather than tethering it by one or more cleavable bonds. In this case, drug release can be regulated by altering the mesh size of the hydrogel network, determined by the distances between crosslinks. As the drug or related cargo moves within the gel network it encounters varying degrees of steric interactions, which is largely dependent on the mesh size.[4] Distances between crosslinks that are much larger than the drug allow for uncontrolled release from the hydrogel dependent only on the intrinsic diffusion properties of the cargo.

Although cleavable linkages have traditionally afforded longer half-lives, degradable cargo-trapping hydrogel systems offer dynamic control of mesh size and thus can achieve systems that can have longer release timeframes with lower burst release.[4] When the distance between crosslinks is smaller than the drug, the drug will essentially be

immobilized within the network until degradation of the network allows the drug to move through the hydrogel and be released. Hydrogels have been engineered to have many different degradation mechanisms, the most common being ester hydrolysis, enzymatic hydrolysis, and photolytic cleavage. Photocleavable linkages offer real-time control over hydrogel degradation for on-demand release. Such examples can be seen in hydrogels with nitrobenzyl moieties which cleave when exposed to 365 nm light.[14,15] However, a major limitation of these systems is that UV light is not able to penetrate deeply into tissue and could also damage healthy cells.[16]

Examples of hydrolytic cleavage mechanisms have included hydrogels made from poly(ethylene glycol) and poly(lactide) to form gels with degradation rates of approximately two weeks.[17,18] Hydrogels made from the crosslinking of hyperbranched poly(β-amino ester)s with thiolated hyaluronic acid were found to have similar stabilities.[19] Hydrogels with enzymatic cleavage mechanisms can exhibit degradation rates over hours or weeks depending on the system and enzyme. For example, hydrogels consisting of dextran and collagen-derived peptides were able to release fluorophores over 16 days in the presence of matrix metalloproteinases.[20] Another example of enzymatic degradation can be seen in functionalized hyaluronan gels with hydrazone crosslinks, which were found to degrade over 40 to 100 hours in the presence of hyaluronidase at physiological pH.[21]

Although these degradation release mechanisms were able to achieve longer release timeframes under mild conditions, they were not easily tunable and required adjustment of crosslinking density, weight percent, and monomer incorporation among other factors to generate different release profiles, making these systems quite complicated. The lack of tunable hydrogel systems is problematic considering that many applications require

different degradation and release properties. For example, hydrogel scaffolds in tissue engineering need to degrade at rates similar to tissue growth whereas injectable depot drug delivery systems for the treatment of certain cancers would ideally have long term release over 6 or 12 months.[22] Consequently, there is a need for hydrogels with highly tunable properties, which can be adapted to fit a wide variety of medical applications.

1.3 Introduction of Oxanorbornadienes

Oxanorbornadienes (ONDs) are the products of the [4+2] cycloaddition of furans with electron-deficient alkynes, and are excellent Michael acceptors toward thiols. Retro-Diels-Alder fragmentation is triggered by thiol addition, yielding the starting furan and thiomaleate (Figure 2).[23] Thiol addition occurs rapidly, and the resulting fragmentation is tunable on the order of hours to months depending on the furan substitution. Extensive studies have been done to explore the rate of this fragmentation process using β-mercaptoethanol-OND adducts with varying OND substitution at the 1 and 4 positions. For example, the addition of a methyl group at the bridgehead carbon of the dimethyl ester OND increased the half-life from 12 hours to 51 hours (Figure 2, R^2=R^3=CO_2Me, R^1=H vs. Me) which could be further increased up to 20 days by the addition of amine derivatives at the same location.[24] Factors proposed as being important in the control of these rates include intramolecular hydrogen bonding (such as between a pendant sulfonamide proton and OND ester group[24]) and the electronic natures and symmetries of the diene and dienophile fragments.[25]

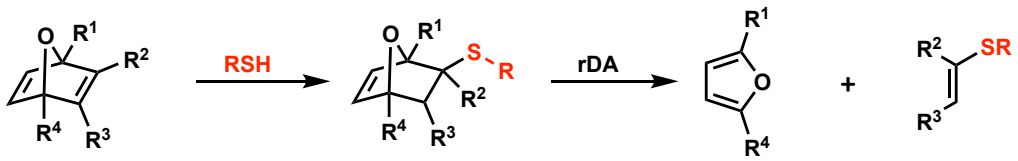

Figure 2. OND thiol addition followed by retro-Diels-Alder fragmentation.

The tunable nature of OND stability has led to the use of these structures as cleavable linkers in drug delivery systems. In one model study, ONDs were explored as linkers that could release cargo from serum albumins at rates between half a day and 7 days depending on the OND substitution pattern.[26] This study, which was done under physiological conditions, highlights the utility of ONDs in complex mixtures. Since the retro-Diels-Alder rate responds mostly to changes in the molecular structure and not to the external conditions, one can have high confidence that performance *in vitro* will predict *in vivo* results.

1.4 Oxanorbornadienes as Cleavable Linkers in Degradable Hydrogels

These properties prompted further investigation of ONDs as cleavable linkages in hydrogel delivery systems. In an initial study, divalent ONDs of different substitution were reacted with tetravalent PEG-thiols to form 10 wt% hydrogels.[27] As predicted, hydrogels made with different ONDs exhibited similar characteristics of swelling and pH insensitivity while having different, pre-programmed, degradation rates. Furthermore, it was found that OND hydrogels were able to release entrained cargo at predictable rates over 6 to 80 hours if the cargo was large enough to be mostly immobilized within the gel network, otherwise

release rates were dependent on diffusion rather than mesh size.[27] A practical drawback of this initial system was that the OND small molecule needed to be dissolved in an aqueous mixture containing DMSO.

Oxanorbornadiene reagents have shown great promise as cleavable linkages in degradable hydrogel systems due to their programmable fragmentation rates, which can be tuned over an exceptionally wide range of time. The unique properties of oxanorbornadienes present an opportunity to create broadly effective drug delivery systems that can be suitable to a wide range of applications without making the hydrogel formulations too complex. The present thesis describes further efforts in the development of OND hydrogels to enhance the biocompatibility of the system and to explore crosslinking composition-property relationships and translation to specific applications.

CHAPTER 2. Development of New Oxanorbornadiene Hydrogels

Oscillatory rheology data presented in this chapter were obtained by Jonas Cuadrado in Dr. Alberto Fernandez-Nieves' lab at the Georgia Institute of Technology.

2.1 Introduction

Current hydrogel delivery systems are able to achieve a wide variety of release timeframes, but this usually requires significant changes in composition. It would be advantageous if the same basic system could be used to make tunable hydrogels that can applied to a variety of problems, without added complexity.

Oxanorbornadiene molecules have been well studied by the Finn lab and were shown to undergo retro-Diels-Alder fragmentation after thiol addition with predictable rates that varied over an extremely wide time range depending on the OND substitution.[23-27] OND hydrogels have previously been explored where a divalent OND small molecule was crosslinked with tetravalent PEG-SH to form degradable hydrogels. OND linkers were used to generate hydrogels with two different release mechanisms, one in which the OND acted as a cleavable bond in the hydrogel network and the other as a cleavable linkage between the network and the cargo. Cleavage of the hydrogel network was shown to be able to release cargo over 6 to 80 hours depending on the OND retro-Diels-Alder rate.[27]

We elaborated on this delivery system by investigating hydrogels where ONDs are coupled onto either dextran or PEG and then crosslinked with PEG or dextran thiols of different valency. Dextran is a water-soluble natural polysaccharide that has been shown

to have low protein absorption.[28] In addition, studies have shown that dextran with molecular weights less than 30,000 are able to be excreted through the kidneys.[29] The incorporation of dextran into the OND hydrogel delivery system was expected to enhance biocompatibility by eliminating the need for DMSO. The properties of these new hydrogel crosslinking compositions were explored as described in the following section.

2.2 Results

2.2.1 Synthesis and fabrication of hydrogels

Oxanorbornadienes were synthesized via Diels-Alder reaction with a commercially available furan and two different substituted alkynes to obtain ONDs with varying stabilities (Figure 3). From previously published kinetic studies, it is expected that methyl ester OND **2** and CF_3 OND **3** will have retro-Diels-Alder half-lives of approximately 18 and 220 days respectively at 25°C.[24] OND **4**, the epoxide of OND **2,** cannot undergo retro-Diels Alder fragmentation and thus can be used to generate non-degradable hydrogels for comparison.[24] ONDs **2-4** were coupled to either dextran (20K) or divalent PEG-amines and then reacted with either tetravalent PEG-SH, divalent PEG-SH, or dextran-SH. For each of the three ONDs, four different crosslinking systems were investigated as outlined in Figure 4. The first three crosslinking systems were dextran-OND with tetravalent PEG-SH, divalent PEG-SH, and dextran-SH. The last crosslinking system explored was divalent PEG-OND with dextran-SH. Experimental details of the synthesis of these materials are outlined in section 2.4.1.

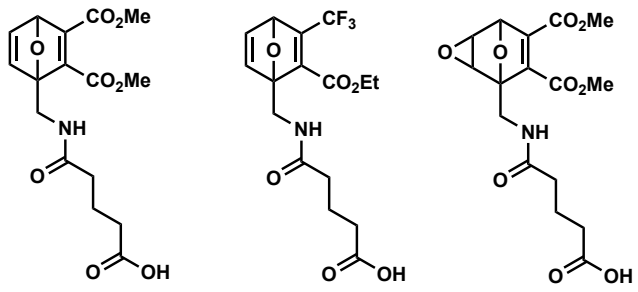

2 3 4

Figure 3. Selected ONDs to be used as degradable (2 and 3) or non-degradable (4) crosslinks in hydrogels.

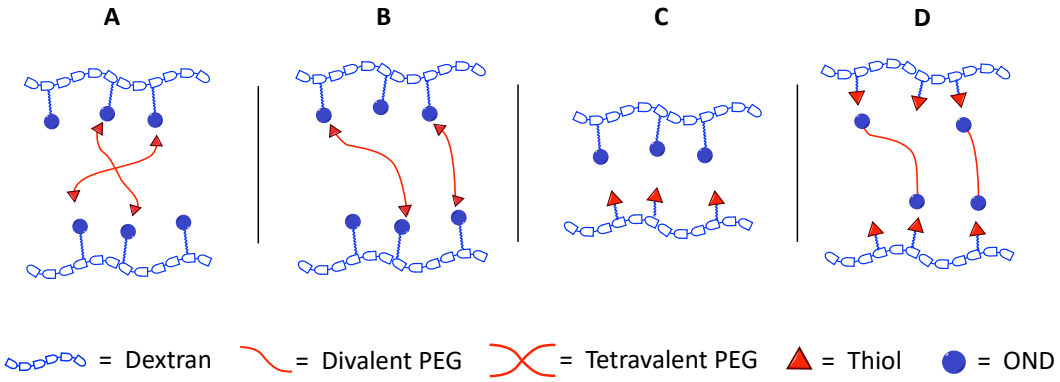

Figure 4. Representation of different hydrogel crosslinking systems that were implemented in OND hydrogels.

Gels were prepared by dissolving OND and thiol material separately in 0.001 M potassium phosphate buffer to make a 10 wt% solution. The OND and thiol materials were then mixed together in a 1-to-1 ratio of thiol to electrophile to form self-supporting 10 wt% gels. The point of gelation was recorded as the time the sample ceased to flow by the inversion test. At room temperature and physiological pH all gels were fully formed in less than 20 seconds.

The rate of gelation could be altered by changing the buffer salt concentration or pH of the solution. Increasing the buffer salt concentration was found to dramatically increase gelation speed and lowering the pH of the hydrogel solutions was found to decrease gelation speed. For example, at pH 5.5 gels took between 2 and 18 minutes to fully form depending on the type of OND and the crosslinking system, with hydrogels made from divalent PEG-SH and dextran-OND taking the longest (2.4.3 Figure 13). Gelation could also be slowed, typically by 30-60 seconds, by cooling the samples on ice.

2.2.2 Swelling ratio and gel fraction determination

The swelling ratio of a hydrogel describes the weight increase of the hydrogel due to water absorption. Swelling ratio has been shown to be linked to the number of crosslinks within the hydrogel network: materials with large numbers of crosslinks are expected to swell less than materials with fewer crosslinks. If swelling ratios are very large then release of entrained and immobilized cargo is less dependent on degradation of the hydrogel network and is instead more dependent on diffusion, which is known to give a burst release profile.[30] Consequently, lower swelling ratios are desirable. The gel fraction of a hydrogel describes the degree to which the starting material was incorporated within the hydrogel network.

Swelling ratios were determined by suspending hydrogels in water and comparing the hydrogel mass after 24 hours to the original hydrogel mass. Gel fractions were determined by lyophilizing hydrogels and comparing the lyophilized mass to the mass of the OND and thiol materials that went into the hydrogel. Further experimental details are outlined in sections 2.4.4 and 2.4.5. The results from swelling and gel fraction studies are

outlined in Table 1. All gels were made as described in the previous section unless otherwise noted.

Table 1. Swelling Ratios and Gel Fractions of selected OND Hydrogels

Entry	Crosslinking System	OND	Swelling Ratio	Gel Fraction
1	A	2	2.2	0.42
2*	A	2	1.2	0.98
3	A	3	3.0	0.84
4	A	4	1.1	0.90
5	B	2	2.6	0.50
6*	B	2	1.5	0.98
7	B	3	2.0	0.72
8	B	4	2.1	0.78
9	C	2	1.4	0.96
10	C	3	1.8	0.92
11	C	4	1.2	0.82
12	D	2	1.7	0.4
13	D	3	3.5	0.86
14	D	4	1.7	0.62

* 5 wt% gels

When comparing crosslinking systems, the dextran-dextran crosslinking system (C) had the lowest swelling ratios and highest gel fractions. Gel fractions for the 4-arm (A) and 2-arm (B) crosslinking systems were also fair with the exception of entries 1 and 5, which both exhibited very poor gel fractions. It was hypothesized that a sufficient number of crosslinks were being formed to make robust hydrogels with only half of the starting material and that very fast gelation could result in the exclusion of excess material from

the bulk hydrogel network. When the experiment was repeated with 5 wt% gels rather than 10 wt% almost all of the material was able to be incorporated within the hydrogel network.

Among ONDs **2**, **3**, and **4**, materials made with OND **3** consistently exhibited the largest swelling ratios. This can be attributed to the lower degree of substitution of OND **3** on dextran (15%) which would result in fewer crosslinks when compared to ONDs **2** and **4** which had 20% and 25% substitution respectively.

2.2.3 Oscillatory rheology

We characterized three different hydrogels by oscillatory rheology in order to investigate how differences in crosslinking might affect their strength and aging properties. The three selected gels were made with methyl ester OND **2** and had the following crosslinking systems: OND-dextran and tetravalent PEG-SH (**2A**), OND-dextran and dextran-SH (**2C**), and OND-PEG and dextran-SH (**2D**). Oscillatory rheology in the linear regime showed that the storage modulus (G'), which describes the elastic behavior of the sample, initially started below the loss modulus (G''), which describes the viscous behavior of the sample, and quickly increased well above G'' until G'' was negligible in comparison. The point where G' crosses over G'' is indicative of gelation and once G' stabilizes the hydrogel is fully formed. The solid-like nature of the selected hydrogels was further confirmed by observing that G' was much greater than G'' at all frequencies and was found to be independent or only weakly dependent on oscillatory frequency (2.4.6 Figure 14).

Storage and loss moduli measurements were continued until G' started to or completely crossed back below G'' at which point the hydrogel had degraded and was no

longer solid-like. As seen in Figure 5, the OND-dextran and tetravalent PEG-SH gel (**2A**) reached a maximum storage modulus of 20 kPa and degraded after approximately 11.5 days. The OND-dextran and divalent PEG-SH gel (**2C**) reached a maximum storage modulus of 3 kPa and degraded after approximately 11.5 days and the OND-PEG and dextran-SH gel (**2D**) reached a maximum storage modulus of 1 kPa and degraded after 2.3 days. Gels **2A** and **2C** both had long aging times where degradation didn't occur until 11.5 days. Gel **2A** had a much larger storage modulus when compared to gel **2B** which can be attributed to larger degrees of crosslinking. The OND-PEG gel (**2D**) had the shortest aging time and the smallest maximum storage modulus. The small storage modulus can be attributed to smaller degrees of crosslinking which aligns with the data from the swelling ratio experiments in the previous section.

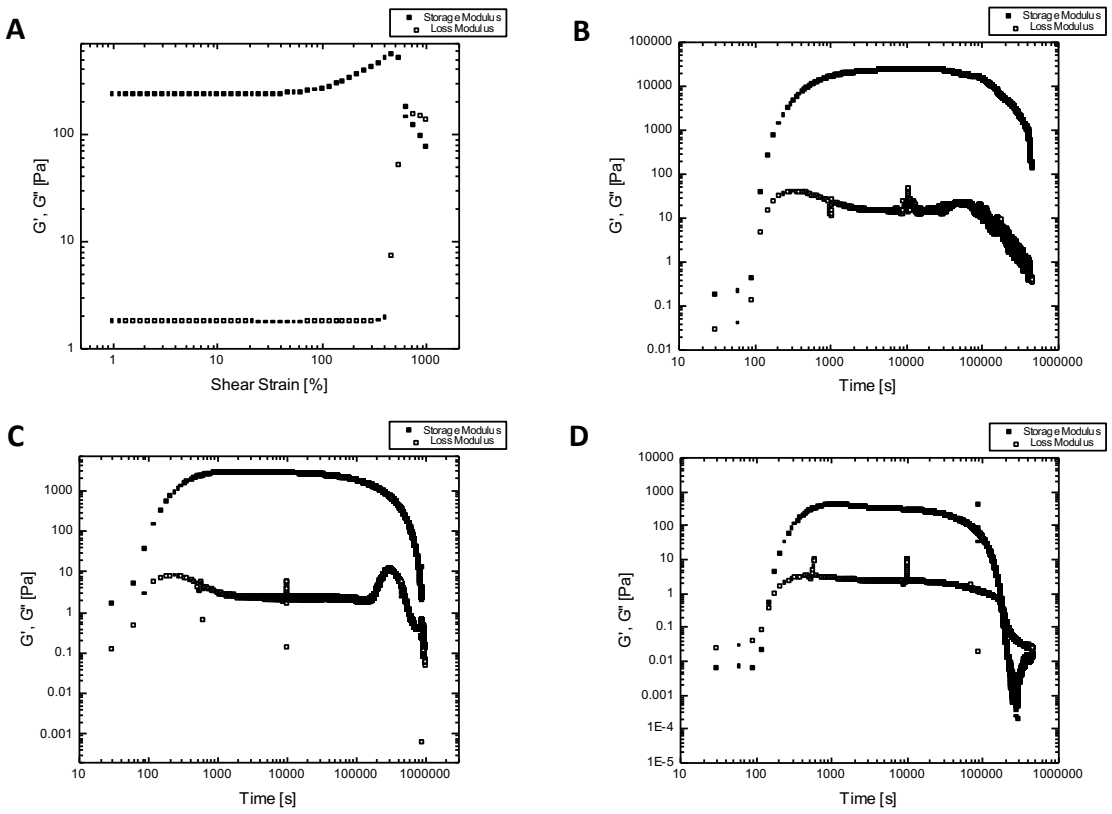

Figure 5. (A) Oscillatory strain sweep of Hydrogel **2D** at an angular frequency of 1 rad/s. (B) Time dependence of G' and G'' for Hydrogel **2A** at a constant strain of 25% and an angular frequency of 1 rad/s. (C) Time dependence of G' and G'' for Hydrogel **2C** at a constant strain of 25% and an angular frequency of 1 rad/s. (D) Time dependence of G' and G'' for Hydrogel **2D** at a constant strain of 25% and an angular frequency of 1 rad/s.

2.2.4 Release studies of entrained Qβ virus-like-particles

Oxanorbornadiene hydrogel delivery systems can deliver cargo through two different strategies, both of which rely on the retro-Diels Alder fragmentation of the OND. The first involves the OND acting as a cleavable linkage between cargo and the hydrogel network while the second implements the OND as a cleavable linkage between the

hydrogel network itself. The second controlled release strategy is dependent on the size of the cargo in relation to the mesh size of the hydrogel network. If the cargo is much smaller than the hydrogel mesh size then release will be entirely dependent on diffusion, which is known to exhibit burst release kinetics.[3, 30] In order to prevent burst release, the entrained cargo must be large enough to be essentially immobilized within the hydrogel network until the network begins to degrade, thus allowing the cargo to move. Qβ virus-like-particles were chosen as a model cargo candidate because of their large size (nearly 30 nm wide) as well as their ability to easily package fluorescent proteins. To examine the release profiles of hydrogels with different ONDs and crosslinking systems, Qβ VLPs were entrained within hydrogels, and release was monitored by fluorescence of the supernatant. Further experimental details are outlined in section 2.4.7.

Release of entrained Qβ cargo from methyl ester OND hydrogels took between 12 and 66 hours depending on the type of crosslinking system (Figure 6). Hydrogel system **2D** (OND-PEG and dextran-SH) took only 12 hours to release 100 percent of entrained cargo, the least amount of time among the four different methyl ester OND hydrogels. While hydrogel **2D** displayed release kinetics similar to burst release, hydrogels **2B** (OND-dextran and divalent PEG-SH) and **2C** (OND-dextran and dextran-SH) had much more linear release curves and took 30 and 42 hours respectively to release 100 percent of entrained Qβ cargo. Hydrogel **2A** (OND-dextran and tetravalent PEG-SH) had the longest release timeline and took 66 hours to release the Qβ-RFP cargo. Although hydrogel **2A** had the longest release profile out of the four different crosslinking systems, the release curve was not linear and instead went through an induction period where there was minimal cargo release for the first 36 hours followed by close to linear release over the next 30 hours.

Since hydrogel **2A** has a high degree of crosslinking, as demonstrated by swelling and oscillatory rheology studies, it is likely that more OND linkages have to break in order for the Qβ cargo to be able to move around within the hydrogel network, which would result in the "induction" period seen in the release curve.

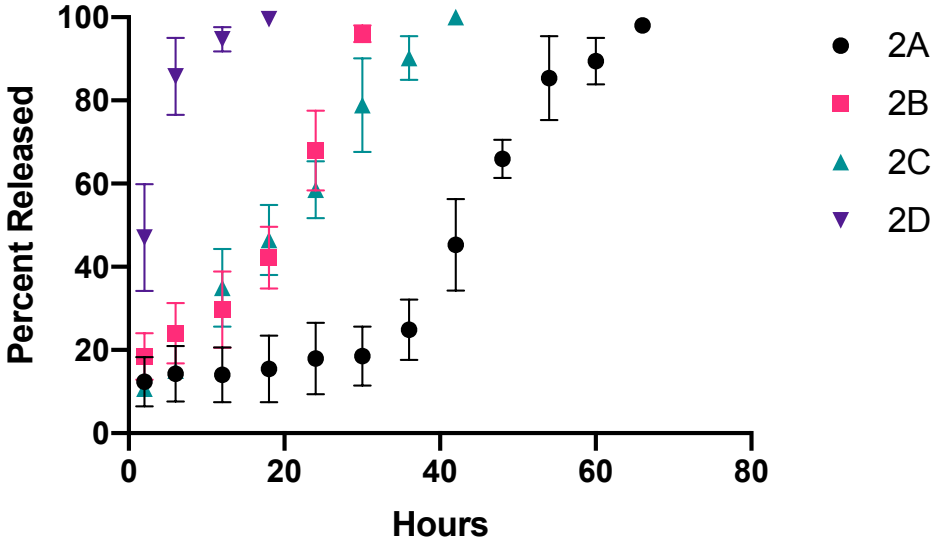

Figure 6. Release of entrained Qβ virus-like particles packaged with RFP from methyl ester OND hydrogels.

Release of entrained Qβ cargo from CF_3 OND hydrogels took between 160 and 600 hours or 6.7 days and 25 days depending on the crosslinking system (Figure 7). Hydrogel **3B** had near linear release kinetics over almost one week, which was the shortest release

timeline of the four different CF_3 gels. Hydrogel **3D** also had near linear release kinetics over 11.5 days while hydrogels **3A** and **3B** had non-linear release kinetics. Hydrogel **3A** went through a similar induction period as seen in the methyl ester OND release study and took almost 18 days to release all of the entrained Qβ cargo. Hydrogel **3C** had the longest release timeline out of any of the gels with 25 days being needed to completely release all cargo, however, release rates were not consistent and exhibited a similar induction period as seen with the 4 arm crosslinking system. In addition, it was observed that the relative degradation rates of 3B and 3D hydrogels were switched in comparison to the degradation rates of 2B and 2D hydrogels. This change can be attributed to differences in the degree of crosslinking of hydrogel samples 2B and 3B. While the degree of crosslinking in hydrogels 2D and 3D can be assumed to be the same, hydrogel 3B had a slightly lower degree of crosslinking than 2B due to differences in OND substitution on dextran (15% and 20% respectively). The reduced substitution of OND 3 in hydrogel 3B most likely resulted in fewer crosslinks being formed which would result in the observed faster degradation.

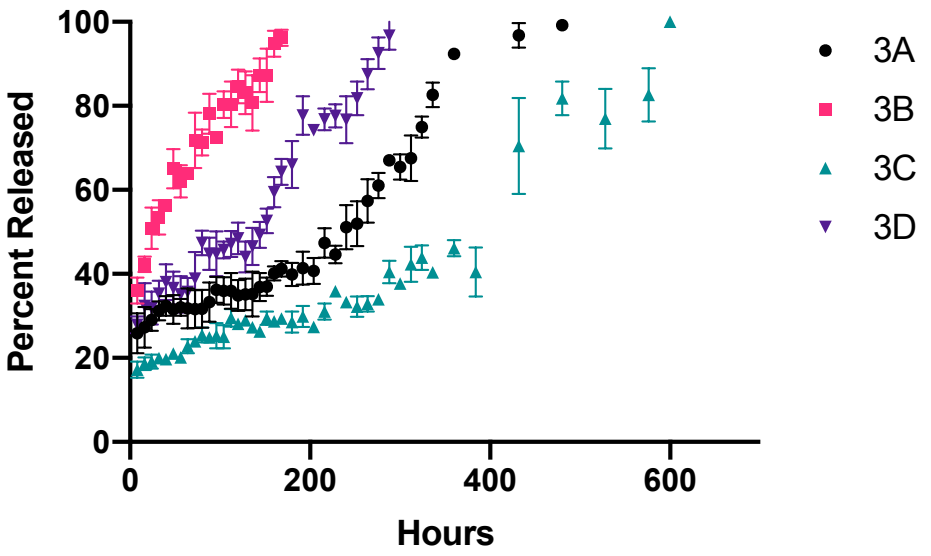

Figure 7. Release of entrained Qβ virus-like particles packaged with RFP from CF_3 OND hydrogels.

In order to validate that the release of Qβ VLPs from OND hydrogel systems was a function of the retro-Diels Alder fragmentation of selected ONDs rather than diffusion or hydrolysis of ester linkages, release experiments were carried out with epoxide ONDs. As stated earlier, epoxide ONDs are not able to undergo cycloreversion and thus can be used to form stable hydrogels that will not degrade by OND cleavage.[24] Consequently, encapsulated Qβ VLPs within epoxide OND hydrogels are not expected to be released. As shown in Figure 8, release of Qβ VLPs from epoxide OND hydrogels with crosslinking systems A-D was stabilized at around 15-25% for over 2 weeks. The initial release of Qβ VLPs seen at the beginning of the experiment is interpreted to be the shedding of VLPs stuck on the surface of the hydrogel rather than VLPs that are encapsulated within the gel. This observation is consistent with the results from the two aforementioned release studies

with methyl ester and CF_3 OND hydrogels. Since there was no detectable release of VLPs from epoxide gels after the initial shedding it can be assumed that release of entrained cargo from the previously mentioned studies was dependent on the cleavage rate of OND linkers.

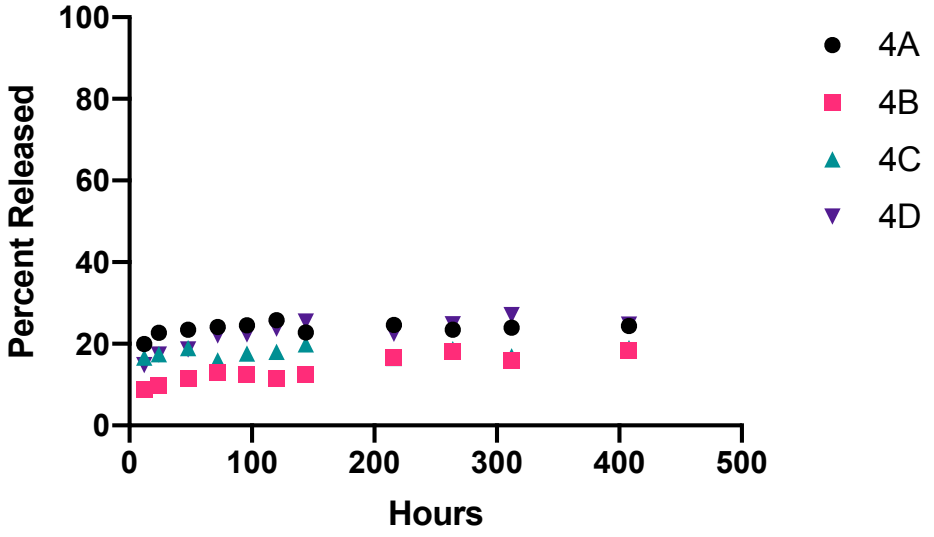

Figure 8. Release of entrained Qβ virus-like particles packaged with RFP from non-degradable epoxide OND hydrogels.

2.3 Conclusion

This work expands the scope of controlled OND hydrogel delivery systems in which a nucleophilic thiol adds to an oxanorbornadiene Michael acceptor rapidly to form network linkages that will undergo tunable retro-Diels-Alder fragmentation.

A library of OND hydrogels with linkages of varying stabilities were synthesized and their release patterns of encapsulated cargo explored. OND hydrogels took only seconds to form robust gels with high material incorporation and low swelling ratios. Release studies of entrained Qβ virus-like-particles packaged with red fluorescent protein demonstrated the tunability of this delivery system where release of cargo was programmed to take as little as 12 hours or as long as 3.5 weeks depending on the OND and crosslinking system. While some crosslinking systems displayed an induction-period followed by steady release, other systems experienced near linear release, which is ideal for hydrogel delivery systems.

Collectively, readily tunable OND hydrogels were achieved through simple alterations of the OND substitution or crosslinking system, which allows them to be broadly useful in a variety of applications, one of which will be discussed in the next chapter.

2.4 Experimental

2.4.1 General information

Reagents and solvents were purchased from commercial sources and used without further purification unless otherwise stated. Water was purified on a Millipore Milli-Q Advantage A10 system. Dextran (20K) was purchased from Alfa Aesar and was dried with toluene prior to use. Divalent and tetravalent PEG-thiols were purchased from JenKem Technologies, USA and were stored in a nitrogen purged glove box. Thiol content was periodically assessed through Ellman's Assay and starting thiol content was found to be 95%. The reactions took place under ambient conditions without any attempt to exclude

air other than capping of the reaction vessel. Flash column chromatography was performed on the Biotage® Automated Liquid Chromatography System Isolera One® using Biotage® SNAP KP-Sil 10 g silica gel cartridges. Analytical thin layer chromatography (TLC) was performed using Whatman glass plates coated with 0.25 mm silica gel and were visualized with UV light and/or potassium permanganate stain. Dye containing compounds were protected from light by aluminum foil.

NMR spectra were obtained using Brüker AMX-400 and DRX-500 instruments in deuterated solvents (Cambridge Isotope Laboratories, Inc.) and were referenced to the solvent. Spectra were processed in MestreNova software (Mestrelab Research). High-resolution mass spectrometry was performed on an Agilent 6230 ESI-TOF LC/MS instrument (G6230B) operating at 4 GHz with internal reference. LC was performed on an Agilent 1260 HPLC with a mobile phase gradient from 0-90% acetonitrile/water containing 0.1% formic acid on a Zorbax Extend-C18 Rapid Resolution HT (2.1 x 50mm, 1.8µm). Absorbance and fluorescence spectra were collected on a VarioskanFlash plate reader (ThermoFisher). Oscillatory rheology measurements were obtained on an Anton Paar Physica MCR 502 rheometer, equipped with an evaporation blocker hood. Measurements were taken using cone-plate geometry and gels were prepared *in situ* with trimming of any excess gel prior to taking measurements.

Synthetic procedures for compounds **1, 2, 3,** and **4** were adapted from previously reported procedures.[24,27] Dextran-SH was synthesized according to literature and the spectroscopic data matched reported values.[31]

2.4.2 Synthetic procedures

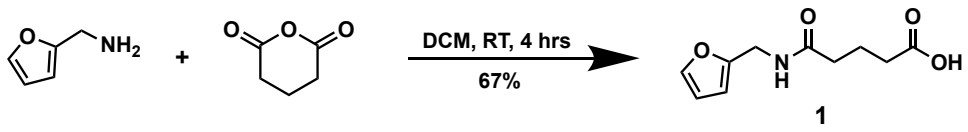

Figure 9. Synthesis of glutaroyl-furfurylamine.

Glutaroyl-furfurylamine: A solution of glutaric anhydride (4g, 35 mmol, 1.7 equiv) in dry DCM (25 mL) was slowly added to a solution of furfurylamine (2g, 20.6 mmol) in dry DCM (20 mL). The resulting solution was stirred for 4 hours at room temperature. The product was filtered, washed with cold DCM, and dried under vacuum (2.9 g, 67% yield). **^{1}H NMR** (400 MHz, Methanol-d_4) δ 7.43 (dd, J = 1.9, 0.9 Hz, 1H), 6.35 (dd, J = 3.3, 1.9 Hz, 1H), 6.25 (dd, J = 3.3, 0.9 Hz, 1H), 4.36 (s, 2H), 2.34 (t, J = 7.4 Hz, 2H), 2.28 (t, J = 7.5 Hz, 2H), 1.95 – 1.85 (m, 2H). **^{13}C NMR** (101 MHz, MeOD) δ 175.36, 173.75, 151.70, 141.86, 109.92, 106.61, 35.70, 34.54, 32.62, 20.81. **HRMS** (ESI-TOF) $C_{10}H_{13}NO_4$ [M + H^+] calcd 212.0923, found 212.0967.

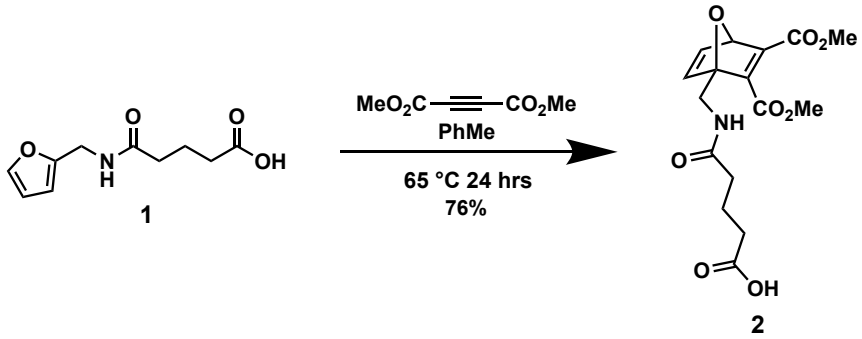

Figure 10. Synthesis of dimethyl ester OND linker.

5-(((2,3-bis(methoxycarbonyl)-7-oxabicyclo[2.2.1]hepta-2,5-dien-1-yl)methyl)amino)-5-oxopentanoic acid: Glutaroyl furfurylamine **1** (1.5 g, 7.1 mmol, 1

equiv) and dimethyl acetylenedicarboxylate (1.51 g, 10.65 mmol, 1.5 equiv) were combined with 1 mL methanol and stirred at 65°C for 20 hours. The resulting solution was triturated against ethyl ether to yield a pale yellow precipitate, filtered, and dried under vacuum (1.9 g, 76% yield). **^{1}H NMR** (400 MHz, Chloroform-*d*) δ 7.23 (dd, *J* = 5.3, 1.9 Hz, 1H), 7.02 (d, *J* = 5.3 Hz, 1H), 6.23 (s, 1H), 5.66 (d, *J* = 1.9 Hz, 1H), 4.18 (dd, *J* = 14.8, 6.3 Hz, 1H), 4.03 (dd, *J* = 14.8, 5.3 Hz, 1H), 3.82 (d, *J* = 14.6 Hz, 6H), 2.41 (t, *J* = 7.1 Hz, 2H), 2.30 (t, *J* = 7.4 Hz, 2H), 1.97 (q, *J* = 7.2 Hz, 2H). **^{13}C NMR** (101 MHz, $CDCl_3$) δ 177.27, 172.72, 163.90, 162.59, 153.43, 152.91, 145.31, 142.91, 96.90, 83.68, 52.64, 52.44, 37.76, 35.04, 32.91, 20.56. **HRMS** (ESI-TOF) $C_{16}H_{19}NO_8$ [M + H$^+$] calcd 354.1189, found 354.1122.

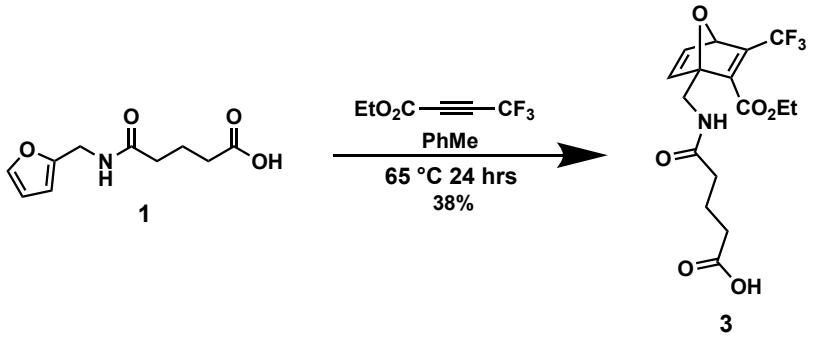

Figure 11. Synthesis of CF_3 OND linker.

5-(((2-(ethoxycarbonyl)-3-(trifluoromethyl)-7-oxabicyclo[2.2.1]hepta-2,5-dien-1-yl)methyl)amino)-5-oxopentanoic acid: Glutaroyl furfurylamine **1 (**1.0 g, 4.7mmol, 1 equiv) and ethyl 4,4,4-trifluoro-2-butynoate (1.18 g, 7.1 mmol, 1.5 equiv) were combined

with 1 mL methanol and stirred at 65°C for 24 hours. The resulting solution was concentrated and triturated against ethyl ether. The off white solid was filtered and dried under vacuum (675 mg, 38% yield). **^{1}H NMR** (400 MHz, Chloroform-*d*) δ 7.21 (dd, *J* = 5.3, 1.9 Hz, 1H), 7.09 (dd, *J* = 5.3, 1.7 Hz, 1H), 5.98 (s, 1H), 5.60 (d, *J* = 1.9 Hz, 1H), 4.36 – 4.22 (m, 2H), 4.22 – 4.04 (m, 2H), 2.46 – 2.35 (m, 2H), 2.35 – 2.21 (m, 2H), 2.04 – 1.89 (m, 2H), 1.33 (t, *J* = 7.1 Hz, 3H). **^{13}C NMR** (101 MHz, $CDCl_3$) δ 176.66, 173.60, 172.55, 172.27, 162.21, 151.78, 151.41, 150.77, 144.59, 143.52, 122.71, 120.03, 96.88, 82.57, 62.16, 62.12, 51.61, 37.66, 37.63, 35.24, 35.06, 32.94, 32.82, 20.75, 20.60, 13.83. **HRMS** (ESI-TOF) $C_{16}H_{18}F_3NO_6$ [M + H^+] calcd, 378.1164, found 378.1101.

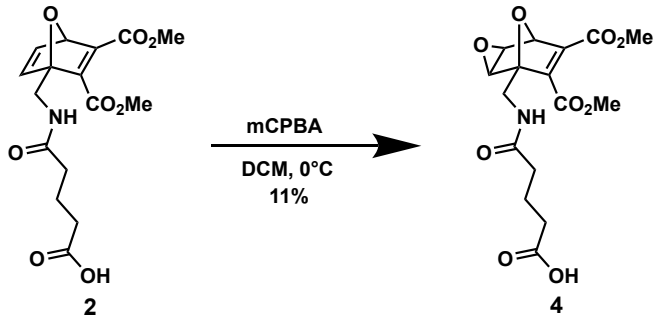

Figure 12. Synthesis of Epoxide OND linker.

5-(((6,7-bis(methoxycarbonyl)-3,8-dioxatricyclo[3.2.1.0^{2,4}]oct-6-en-1-yl)methyl)amino)-5-oxopentanoic acid: meta-Chloroperoxybenzoic acid (335 mg, 1.36 mmol, 1.2 equiv) was added to a solution of OND **1** (400 mg, 1.13 mmol, 1 equiv) in 12 mL DCM. The solution was stirred on ice overnight. The crude product was purified by

flash chromatography on silica gel with a gradient of ethyl acetate through 20% MeOH/EtOAc to yield a white solid (45 mg, 11% yield). **^{1}H NMR** (400 MHz, Chloroform-*d*) δ 6.08 (s, 1H), 5.13 (s, 1H), 4.05 (d, *J* = 5.8 Hz, 2H), 3.86 (d, *J* = 16.4 Hz, 6H), 3.83 – 3.74 (m, 2H), 2.45 (t, *J* = 7.0 Hz, 2H), 2.36 – 2.29 (m, 2H), 2.04 – 1.96 (m, 2H). ^{13}C NMR (101 MHz, $CDCl_3$) δ 177.07, 172.77, 162.89, 161.82, 149.50, 146.83, 91.15, 78.34, 57.14, 56.43, 52.96, 52.73, 37.02, 34.95, 32.82, 20.50. **HRMS** (ESI-TOF) $C_{16}H_{19}NO_9$ [M + H^+] calcd 370.1138, found 370.1101.

General procedure A: OND-Dextran coupling:

Dextran 20K (334 mg, 2.0 mmol, 1 equiv) and lithium chloride (600 mg, 14 mmol, equiv) were added to 30 mL DMF and stirred at 90°C for 30 minutes. The resulting solution was cooled to 0°C and N,N'Dicyclohexylcarbodiimide (518 mg, 2.5mmol, 1.25 equiv), OND **2, 3, or 4** (0.4 equiv), and 4-(dimethylamino)pyridinium 4-toluenesulfonate (77.5 mg, 0.27 mmol, 0.14 equiv) were added to the cooled solution under stirring. The resulting solution was stirred at 4°C for 3 days, after which the solution was filtered through a 0.2 μm syringe filter and subsequently precipitated in 150 mL acetone under stirring. The white precipitate was collected by vacuum filtration, rehydrated in 9 mL water, and dialyzed (MW cutoff 3500 Da) against water for 2 days at 4°C. The solution was filtered, frozen, and lyophilized to yield a white fluffy powder. Theoretical OND substitution 40%.

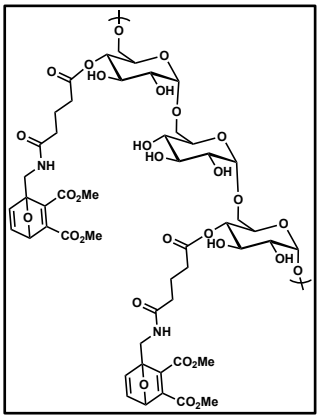

ME OND DEX: Synthesized according to General Procedure A. Experimental substitution 18-25%. **^{1}H NMR** (400 MHz, Deuterium Oxide) δ 7.42 – 7.32 (m, 1H), 7.18 (d, *J* = 5.2 Hz, 1H), 5.87 – 5.74 (m, 1H), 5.18 (s, 1H), 5.01 (d, *J* = 4.5 Hz, 3H), 4.32 (s, 2H), 4.08 – 3.92 (m, 7H), 3.86 (d, *J* = 14.5 Hz, 6H), 3.68 – 3.49 (m, 7H), 2.52 (s, 2H), 2.34 (s, 2H), 1.93 (s, 2H). **^{13}C NMR** (126 MHz, D_2O) δ 174.29, 165.05, 163.65, 153.61, 153.06, 145.15, 142.15, 97.46, 96.84, 83.45, 73.15, 71.16, 69.94, 69.26, 65.26, 52.89, 52.73, 37.13, 34.23, 32.85, 32.58, 20.48.

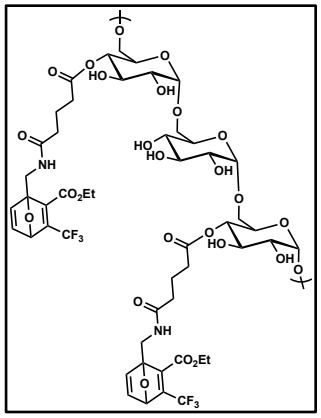

CF3 OND DEX: Synthesized according to General Procedure A. Experimental substitution 15%. **^{1}H NMR** (400 MHz, Deuterium Oxide) δ 7.41 (s, 1H), 7.24 (s, 1H), 6.41 (d, *J* = 43.4 Hz, 1H), 5.89 (s, 1H), 5.01 (d, *J* = 3.8 Hz, 11H), 4.46 – 4.20 (m, 4H), 4.07 – 3.88 (m, 21H), 3.82 – 3.70 (m, 21H), 3.64 – 3.51 (m, 18H), 2.52 (s, 2H), 2.34 (s, 2H), 1.93 (s, 2H), 1.34 (d, *J* = 7.0 Hz, 3H). **^{13}C NMR** (126 MHz, D_2O) δ 175.66, 144.80, 142.48, 97.45, 97.00, 82.32, 73.14, 72.83, 72.67, 71.57, 71.15, 69.92, 69.26, 65.26, 63.04, 62.18, 60.21, 37.05, 34.22, 32.54, 20.49, 12.93.

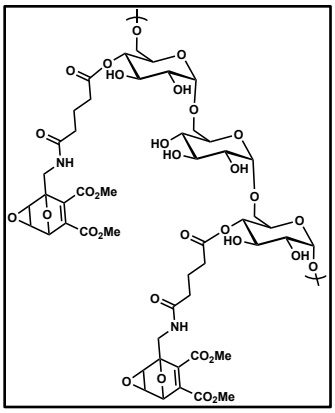

Epoxide OND DEX: Synthesized according to General Procedure A. Experimental substitution 25%. **^{1}H NMR** (500 MHz, Deuterium Oxide) δ 5.48 (s, 1H), 5.35 (s, 1H), 5.18 (d, *J* = 4.7 Hz, 3H), 4.37 (s, 1H), 4.30 (s, 1H), 4.25 – 4.10 (m, 7H), 4.09 – 4.04 (m, 6H), 4.00 – 3.88 (m, 7H), 3.82 – 3.68 (m, 5H), 3.18 (dd, *J* = 19.0, 2.9 Hz, 1H), 2.70 (d, *J* = 7.4 Hz, 2H), 2.53 (t, *J* = 7.2 Hz, 2H), 2.16 – 2.06 (m, 2H). **^{13}C NMR** (126 MHz, D_2O) δ 174.57, 164.23, 163.16, 148.77, 148.04, 97.77, 91.18, 78.34, 73.44, 71.45, 70.24, 69.63, 65.69, 57.60, 56.68, 53.35, 53.20, 36.58, 34.49, 33.01, 32.88, 20.64.

General Procedure B: OND-PEG Coupling

OND **2, 3,** or **4** (2.5 equiv.) was dissolved in 1.5 mL of DMF. HATU (52 mg, 0.14 mmol, 3 equiv) and N,N-Diisopropylethylamine (29.2 mg, 0.23 mmol, 5 equiv.) were added to the OND solution followed by addition of PEG(Amine)2, HCl Salt (225 mg, 0.045 mmol, 1 equiv). The reaction was stirred at room temperature for 2-4 hours followed by precipitation in ether. The off-white solid was collected by vacuum filtration, rehydrated in 1 mL of water, and dialyzed (MW cutoff 3500 Da) against water for 2 days. The retentate was filtered, frozen, and lyophilized to yield a white fluffy powder.

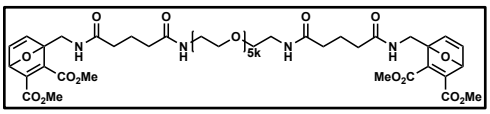

ME OND PEG: Synthesized according to General Procedure B. **^{1}H NMR** (400 MHz, Deuterium Oxide) δ 7.39 (dd, *J* = 5.3, 2.1 Hz, 2H), 7.18 (d, *J* = 5.3 Hz, 2H), 5.84 (d, *J* = 2.0 Hz, 2H), 4.34 (d, *J* = 15.2 Hz, 4H), 3.86 (d, *J* = 13.0 Hz, 12H), 3.73 (s, 605H), 3.65 (t, *J* = 5.4 Hz, 6H), 3.56 (d, *J* = 4.5 Hz, 2H), 3.42 (t, *J* = 5.4 Hz, 4H), 2.29 (t, *J* = 7.5 Hz, 8H), 1.93 – 1.85 (m, 4H). **^{13}C NMR** (126 MHz, D_2O) δ 175.55, 175.46, 165.12, 163.67, 153.58, 153.13, 145.13, 142.09, 96.89, 83.44, 69.42, 69.36, 69.27, 69.17, 68.58, 52.85, 52.69, 38.67, 37.07, 34.55, 34.34, 21.50.

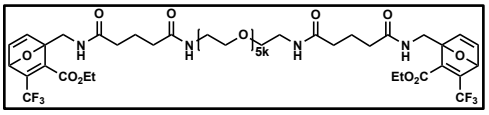

CF3 OND PEG: Synthesized according to General Procedure B. **^{1}H NMR** (500 MHz, Deuterium Oxide) δ 7.39 (dd, *J* = 5.3, 2.1 Hz, 2H), 7.22 (d, *J* = 5.3 Hz, 2H), 5.86 (d, *J* = 2.0 Hz, 2H), 4.39 – 4.26 (m, 8H), 3.84 (t, *J* = 2.4 Hz, 4H), 3.71 (s, 701H), 3.62 (t, *J* = 5.4 Hz, 6H), 3.57 – 3.55 (m, 2H), 3.39 (t, *J* = 5.3 Hz, 4H), 2.26 (dt, *J* = 7.6, 3.9 Hz, 8H), 1.88 – 1.84 (m, 4H), 1.31 (d, *J* = 7.2 Hz, 6H). **^{13}C NMR** (126 MHz, D_2O) δ 175.51, 175.46, 163.68, 151.26, 150.46, 144.80, 142.49, 97.05, 82.31, 69.41, 69.35, 69.17, 68.58, 63.04, 54.11, 51.93, 38.67, 36.99, 34.55, 34.34, 21.56, 12.88.

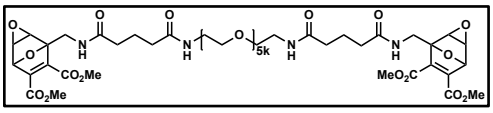

Epoxide OND PEG: Synthesized according to General Procedure B. **^{1}H NMR** (500 MHz, Deuterium Oxide) δ 5.29 (s, 2H), 4.21 (d, *J* = 15.3 Hz, 2H), 4.07 (dd, *J* = 34.1, 3.7 Hz, 4H), 3.87 (s, 6H), 3.84 (s, 6H), 3.83 (d, *J* = 2.5 Hz, 4H), 3.71 (s, 823H), 3.62 (d, *J* = 5.3 Hz, 6H), 3.56 (dd, *J* = 4.2, 2.0 Hz, 4H), 3.38 (d, *J* = 5.4 Hz, 4H), 2.28 – 2.25 (m, 8H), 1.86 (s, 4H). **^{13}C NMR** (126 MHz, D_2O) δ 175.58, 175.52, 164.06, 162.89, 148.59, 147.87, 91.01, 78.09, 69.41, 69.35, 69.27, 69.17, 68.57, 57.44, 56.42, 53.05, 52.88, 38.67, 36.27, 34.53, 34.31, 21.47.

2.4.3 General hydrogel preparation

Hydrogels were prepared by first dissolving the OND material and thiol material separately in 0.001 M potassium phosphate buffer and then combining the two solutions in a 1:1 ratio of OND to thiol. Gelation was determined to be complete by the inversion test when the gel material was observed to be no longer flowing. Once the OND and thiol solutions were mixed, the hydrogels were formed in as little as 2 seconds. Gelation times could be tuned as a function of pH or buffer concentration. It was found that increasing the buffer concentration sped up gelation significantly and that decreasing the buffer pH could slow down gelation. Hydrogels prepared in 7 to 8 pH buffers all took less than 20 seconds to gel, whereas most hydrogels prepared in buffers at pH 5.5-7 were still able to form gels but took as long as 18 minutes to form self-supporting gels. Gels reported were prepared as 10 wt% gels in 0.001 M potassium phosphate buffer, however, gelation could be achieved at ratios as low as 2.5 wt%.

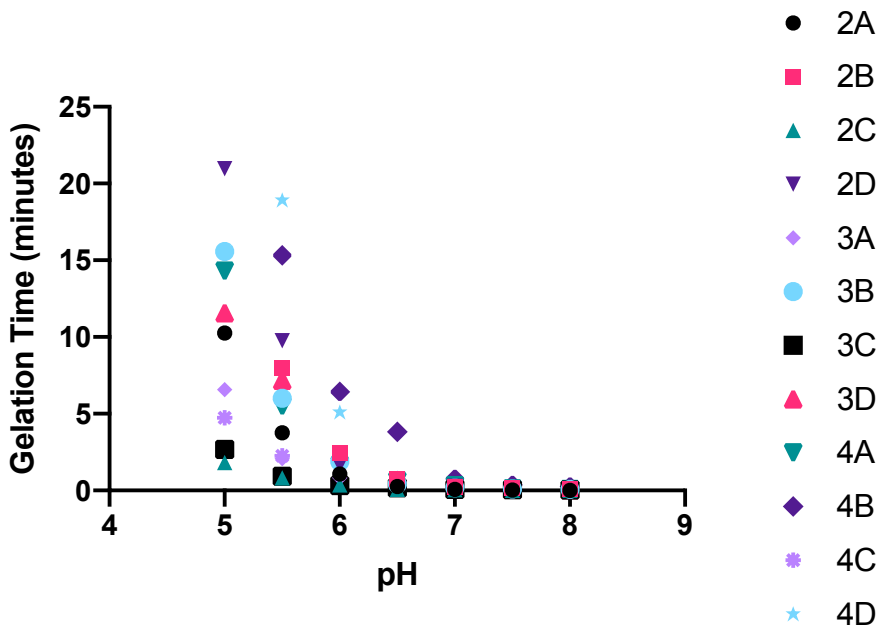

Figure 13. Dependence of pH on gelation time for hydrogels with different crosslinking compositions.

2.4.4 Determination of swelling ratio

50 µL 10 wt% gels were prepared in 0.001 M potassium phosphate buffer in a 1:1 ratio of OND to thiol as described above. The gels were allowed to cure for 5 minutes at room temperature, weighed (M_0), and then suspended in 1 mL of DI water. The gels were stored at 4 °C to prevent significant degradation of the hydrogel network. Hydrogel swelling was monitored periodically by decanting, gently wiping any excess water off of the gel, and weighing. After 24 hours, when swelling had reached equilibrium, the masses of the gels were recorded as M_{eq}.

$$Equilibrium\ Mass\ Swelling\ Ratio = \frac{M_{eq}}{M_0} \quad (1)$$

2.4.5 Determination of gel fraction

Once the equilibrium mass swelling ratio was determined, the gels were frozen, lyophilized and weighed (M_{res}). The ratio of the residual gel mass to the mass of OND and thiol materials that went into making the gel (M_{in}), provided the fraction of gel material that was incorporated within the gel network. Any salts present in the gel were expected to be removed through exchanging the swelling solvent (DI water).

$$Gel\ Fraction = \frac{M_{res}}{M_{in}} \quad (2)$$

2.4.6 Oscillatory rheology

The viscoelastic properties of different Dextran-OND and PEG-OND gels were assessed using oscillatory rheology. 100 μL 10 wt% gels were prepared in 0.001 M potassium phosphate buffer in a 1:1 ratio. The solution was quickly mixed and then dispensed onto the center of the rheometer plate. The cone was brought into contact with the gel and any excess gel was trimmed. The storage (G') and loss (G'') moduli were then measured overtime at a constant strain of 25% and an angular frequency of 1 rad/s to monitor the aging of the gels. It was found that gel samples had a linear response at a wide range of strains as seen in Figure 5A. Frequency sweeps in this linear region for the different gels showed that there was only a weak frequency dependence as seen in Figure 14. All gel samples exhibited a sharp increase of G' over G'' indicating gelation. G' continued to increase until G'' was negligible in comparison. This combined with strain and frequency sweeps confirmed the solid-like nature of the gel. Storage and loss moduli measurements were continued until G' crossed back to below G'' indicating that the gel was more liquid like and had degraded.

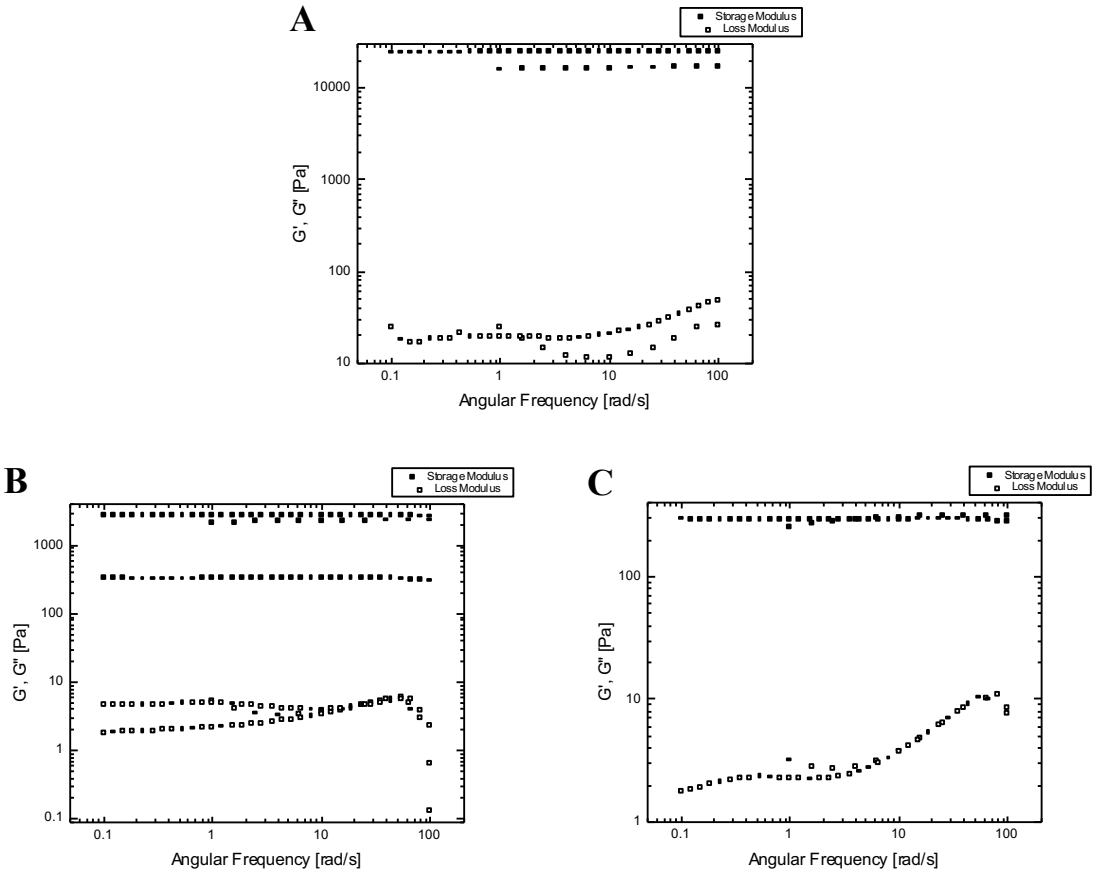

Figure 14. Frequency sweeps for hydrogels with crosslinking compositions (A) 2A (B) 2C (C) 3D.

2.4.7 Release of entrained cargo

Qβ virus-like-particles were prepared by Dr. Soumen Das in the Finn lab. To make 100 μL 10 wt% gels, separate vials of OND and thiol material were dissolved in a 5.5 mg/ml solution of Qβ virus-like-particles in 0.001 M potassium phosphate buffer. The OND and thiol solutions were put on ice for 1 minute. The thiol solution was added to the OND solution, the mixture was pipetted up and down and then transferred to molds. The gels were allowed to cure for 5 minutes and then were removed from their molds, transferred to vials, and suspended in 800 μL of deionized water. The gels were incubated at 37°C and release of RFP packaged QB in the supernatant was monitored by fluorescence with excitation and emission at 585 nm and 605 nm respectively. All four crosslink systems for each type of OND were tested and methyl ester OND and CF3 OND systems were done in triplicate.

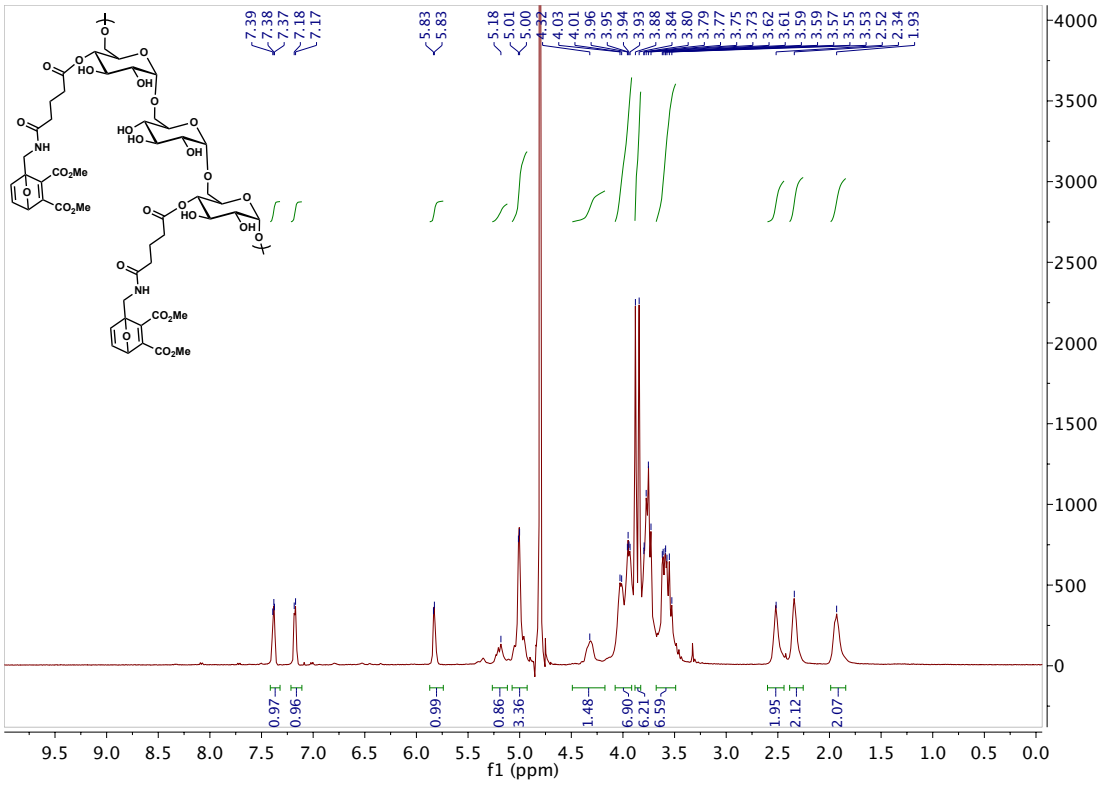
7.39
7.38
7.37
7.18
7.17
5.83
5.83
5.18
5.01
5.00
4.32
4.03
4.01
3.96
3.95
3.94
3.93
3.88
3.84
3.80
3.79
3.77
3.75
3.73
3.62
3.61
3.59
3.59
3.57
3.55
3.53
2.52
2.34
1.93
0.97
0.96
0.99
0.86
3.36
1.48
6.90
6.21
6.59
1.95
2.12
2.07
f1 (ppm)

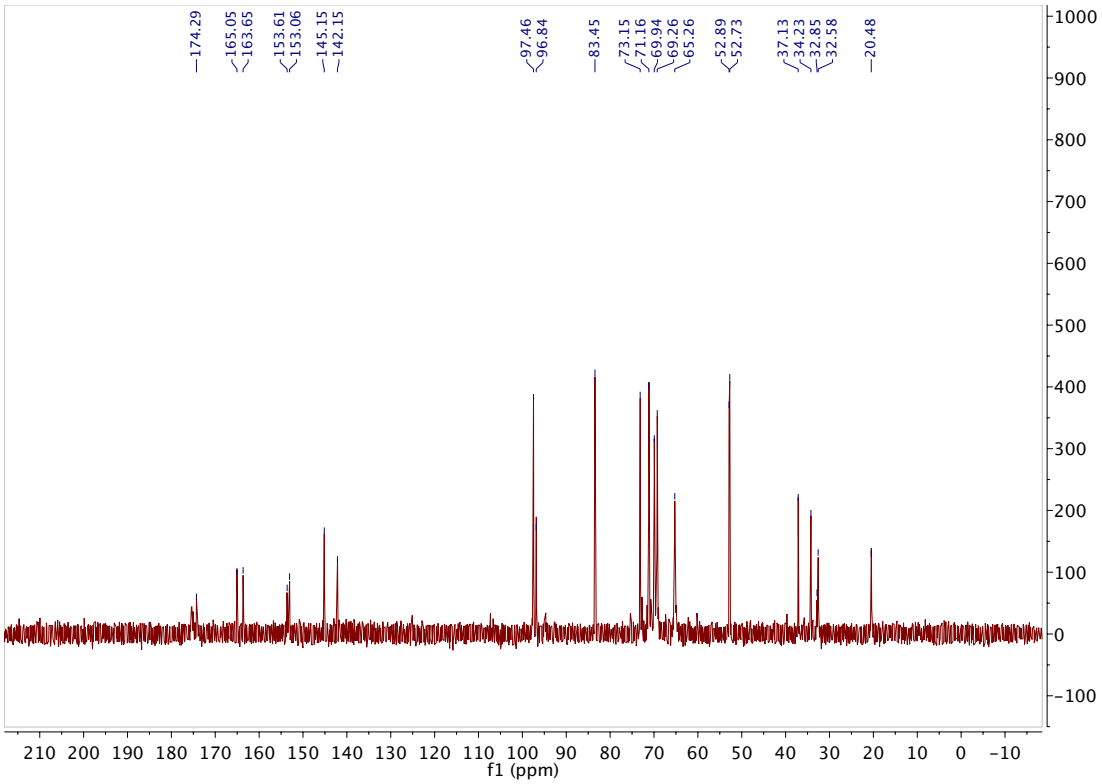
174.29
165.05
163.65
153.61
153.06
145.15
142.15
97.46
96.84
83.45
73.15
71.16
69.94
69.26
65.26
52.89
52.73
37.13
34.23
32.85
32.58
20.48
f1 (ppm)

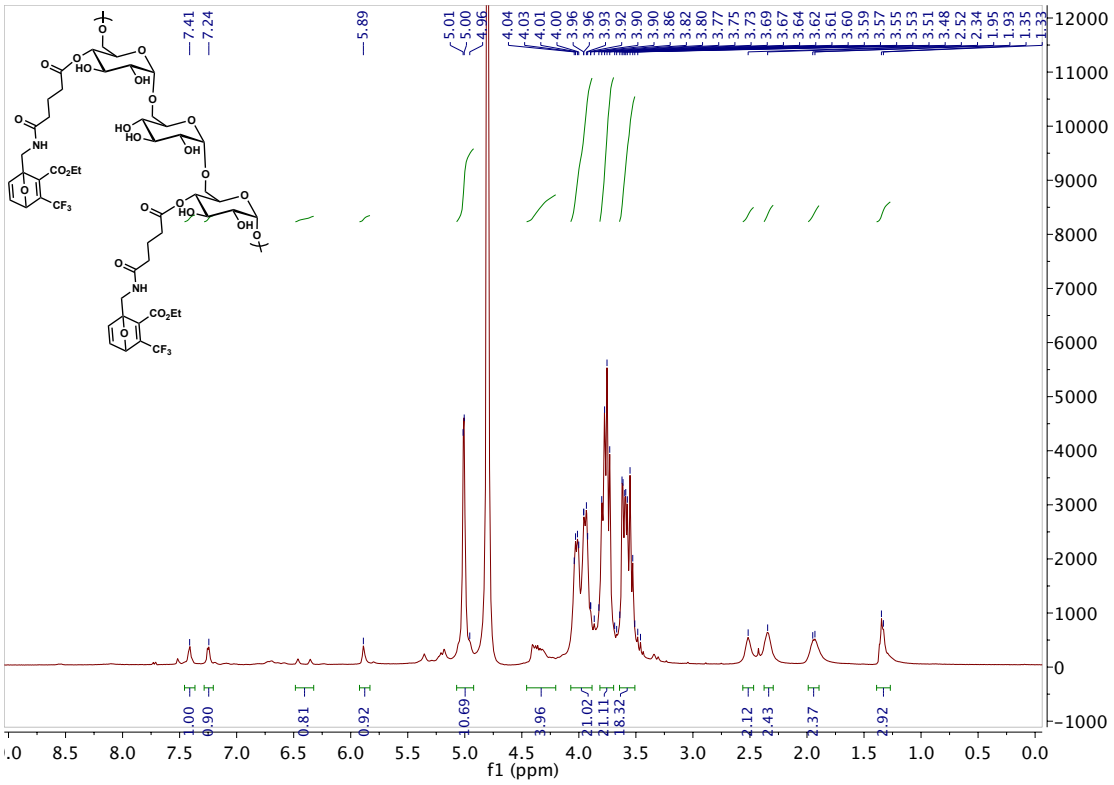
7.41
7.24
5.89
5.01
5.00
4.96
4.04
4.03
4.01
4.00
3.96
3.96
3.93
3.92
3.90
3.90
3.86
3.82
3.80
3.77
3.75
3.73
3.69
3.67
3.64
3.62
3.61
3.60
3.59
3.57
3.55
3.53
3.51
3.48
2.52
2.34
1.95
1.93
1.35
1.32
1.00
0.90
0.81
0.92
10.69
3.96
21.02
21.11
18.32
2.12
2.43
2.37
2.92
f1 (ppm)

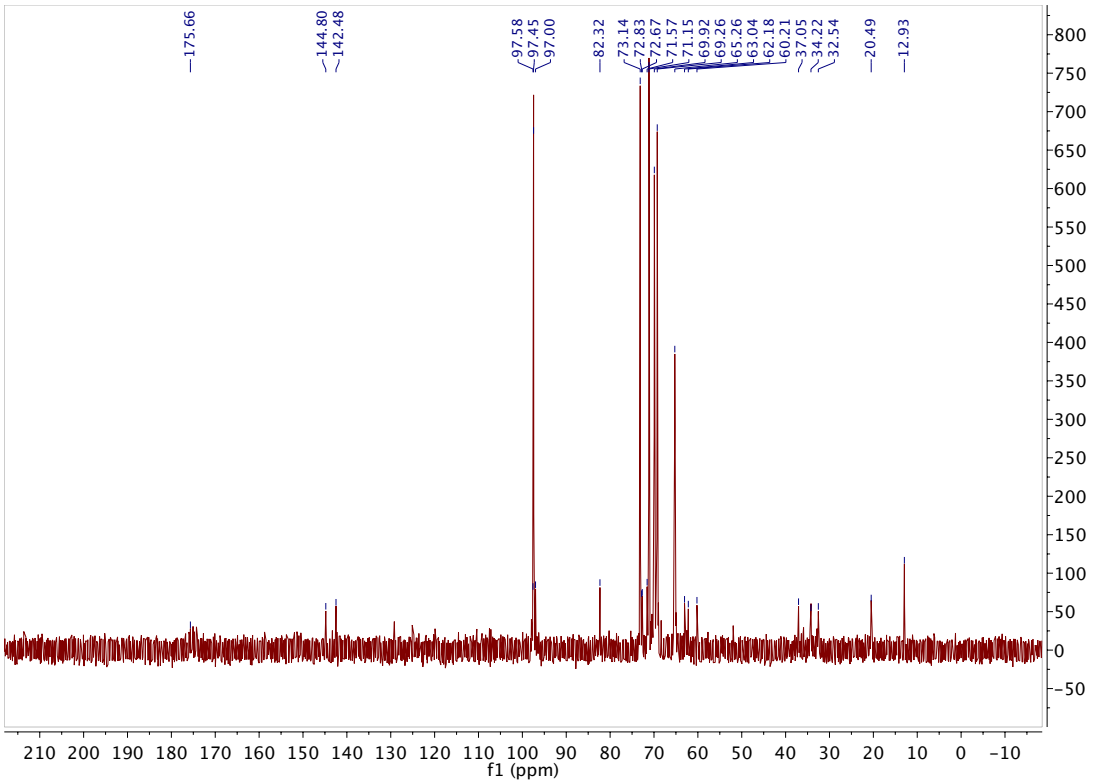
175.66
144.80
142.48
97.58
97.45
97.00
82.32
73.14
72.83
72.67
71.57
71.15
69.92
69.26
65.26
63.04
62.18
60.21
37.05
34.22
32.54
20.49
12.93
f1 (ppm)

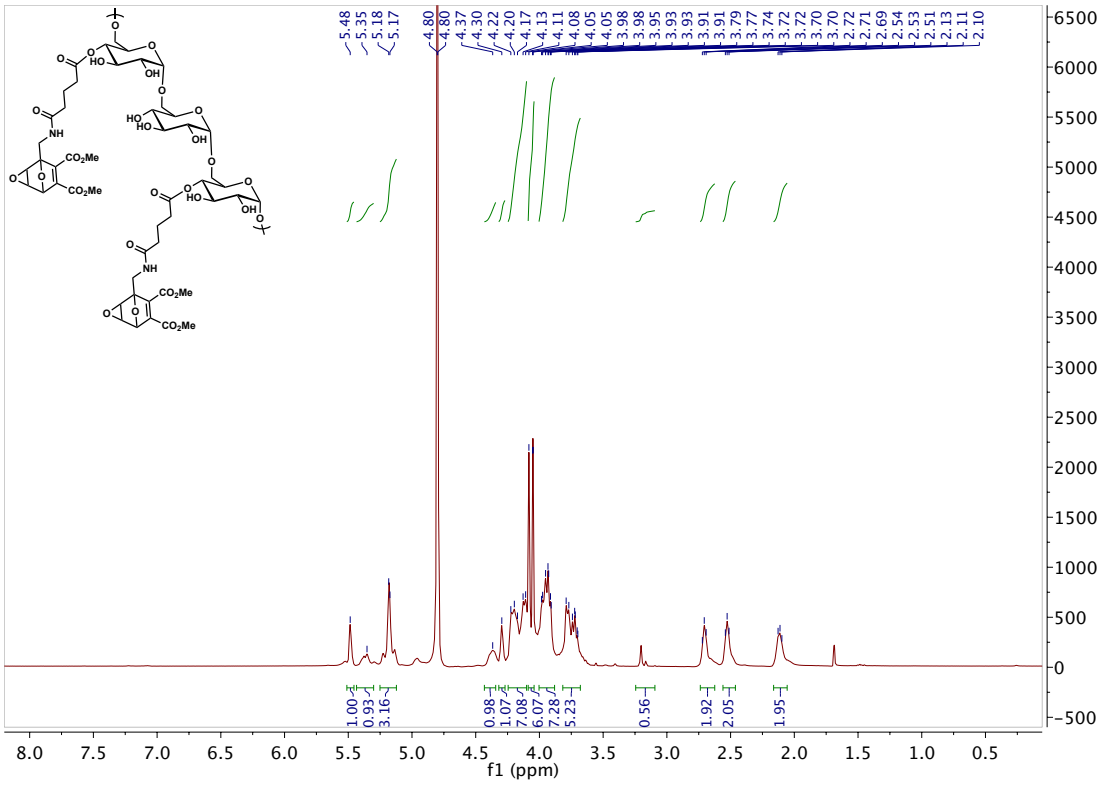
5.48
5.35
5.18
5.17
4.80
4.80
4.37
4.30
4.22
4.20
4.17
4.13
4.11
4.08
4.05
4.05
3.98
3.98
3.95
3.93
3.93
3.91
3.91
3.79
3.77
3.74
3.72
3.72
3.70
3.70
2.72
2.71
2.69
2.54
2.53
2.51
2.13
2.11
2.10
1.00
0.93
3.16
0.98
1.07
7.08
6.07
7.28
5.23
0.56
1.92
2.05
1.95
f1 (ppm)

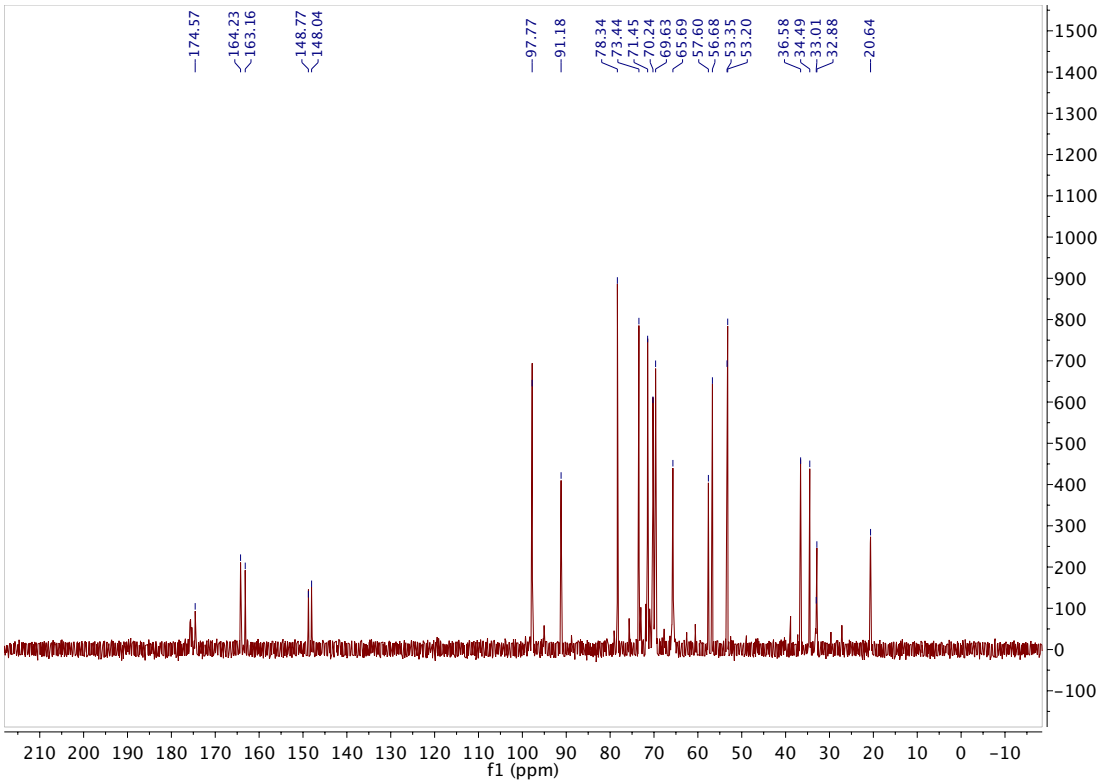
174.57
164.23
163.16
148.77
148.04
97.77
91.18
78.34
73.44
71.45
70.24
69.63
65.69
57.60
56.68
53.35
53.20
36.58
34.49
33.01
32.88
20.64
f1 (ppm)

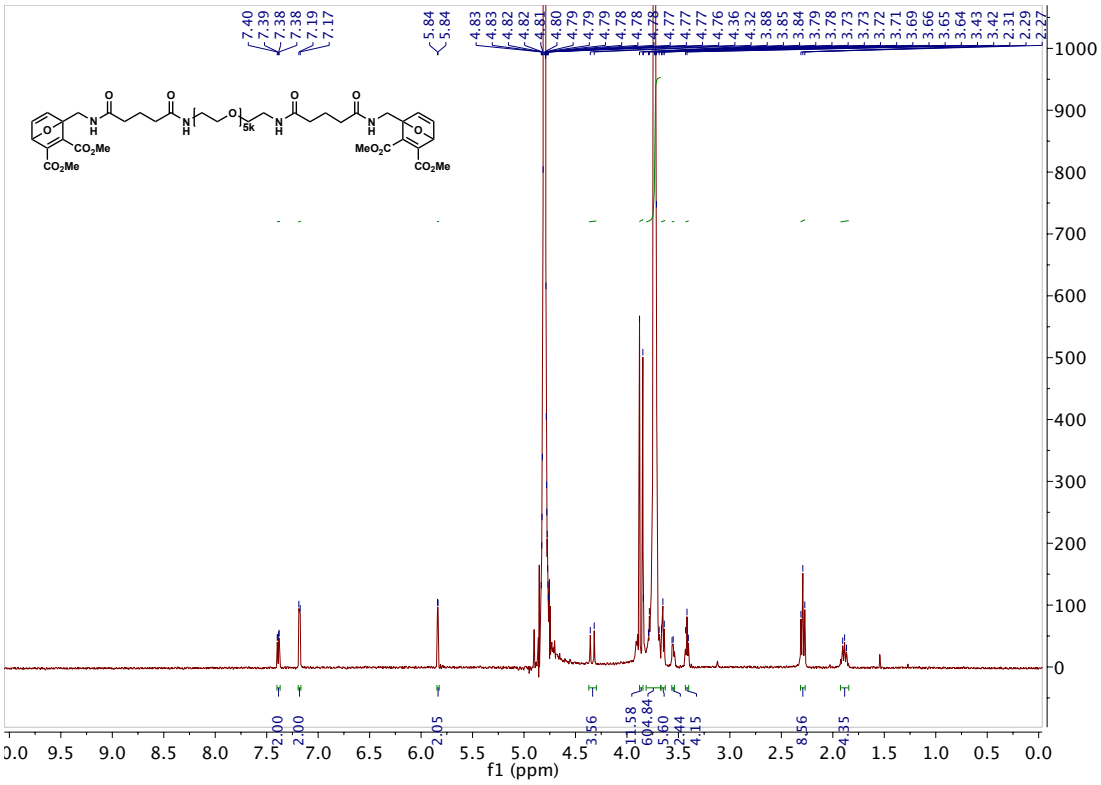
7.40
7.39
7.38
7.38
7.19
7.17
5.84
5.84
4.83
4.83
4.82
4.82
4.81
4.80
4.79
4.79
4.78
4.78
4.78
4.77
4.77
4.77
4.76
4.36
4.32
3.88
3.85
3.84
3.79
3.78
3.73
3.73
3.72
3.71
3.69
3.66
3.65
3.64
3.43
3.42
2.31
2.29
2.27
CO2Me
CO2Me
MeO2C
CO2Me
5k
2.00
2.00
2.05
3.56
11.58
604.84
5.60
2.44
4.15
8.56
4.35
f1 (ppm)

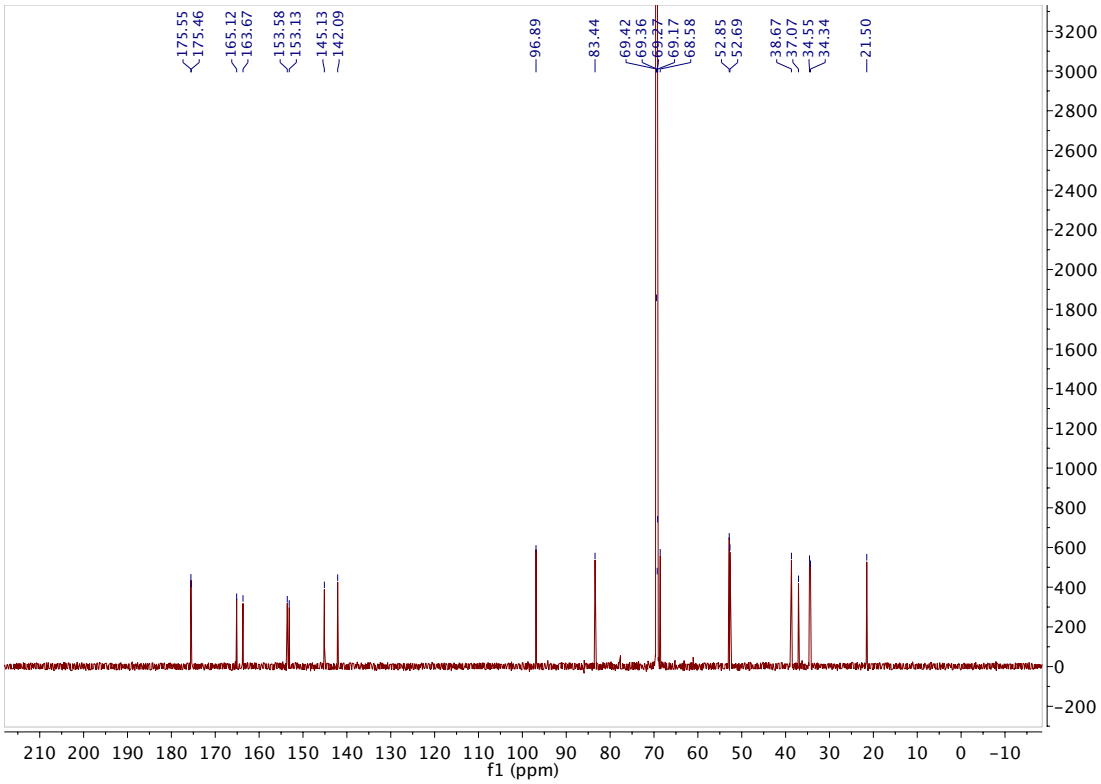
175.55
175.46
165.12
163.67
153.58
153.13
145.13
142.09
96.89
83.44
69.42
69.36
69.27
69.17
68.58
52.85
52.69
38.67
37.07
34.55
34.34
21.50
f1 (ppm)

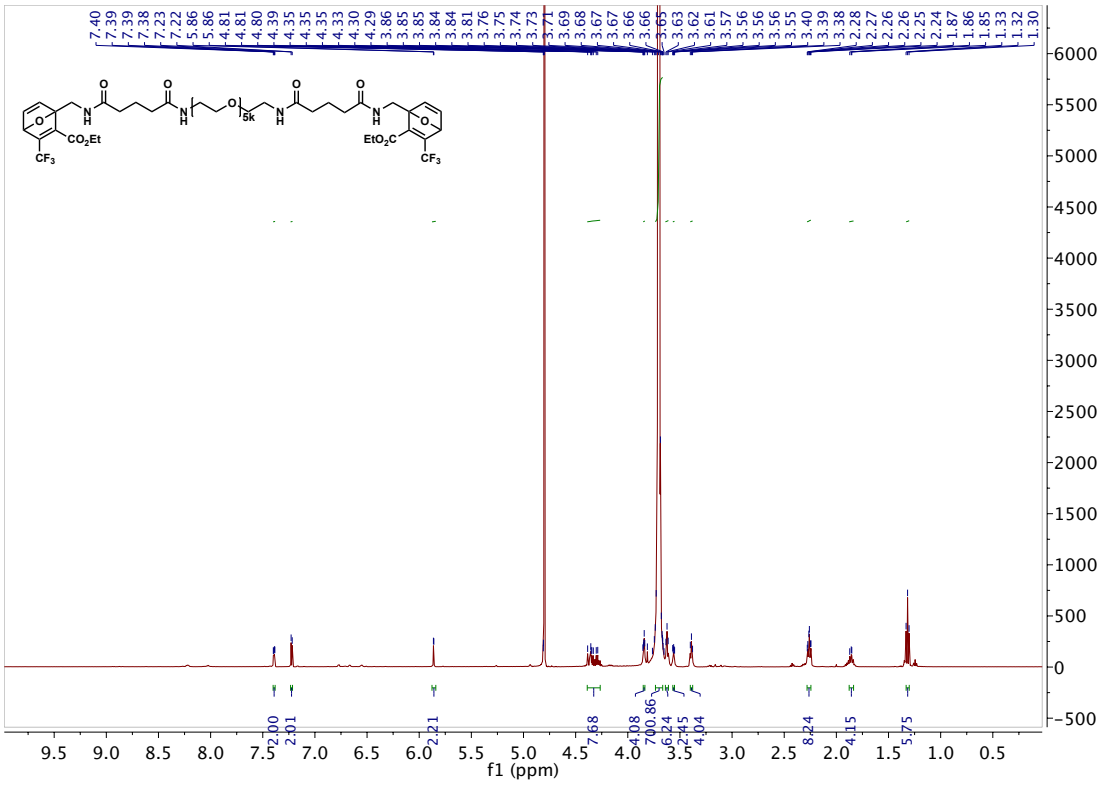
7.40 7.39 7.39 7.38 7.23 7.22 5.86 5.86 4.81 4.81 4.80 4.39 4.35 4.35 4.35 4.33 4.30 4.29 3.86 3.85 3.85 3.84 3.84 3.81 3.76 3.75 3.74 3.73 3.71 3.69 3.68 3.67 3.67 3.66 3.66 3.65 3.63 3.62 3.61 3.57 3.56 3.56 3.56 3.55 3.40 3.39 3.38 2.28 2.27 2.26 2.26 2.25 2.24 1.87 1.86 1.85 1.33 1.32 1.30
CO2Et
CF3
5k
EtO2C
CF3
2.00 2.01 2.21 7.68 4.08 7.00.86 6.24 2.45 4.04 8.24 4.15 5.75
f1 (ppm)

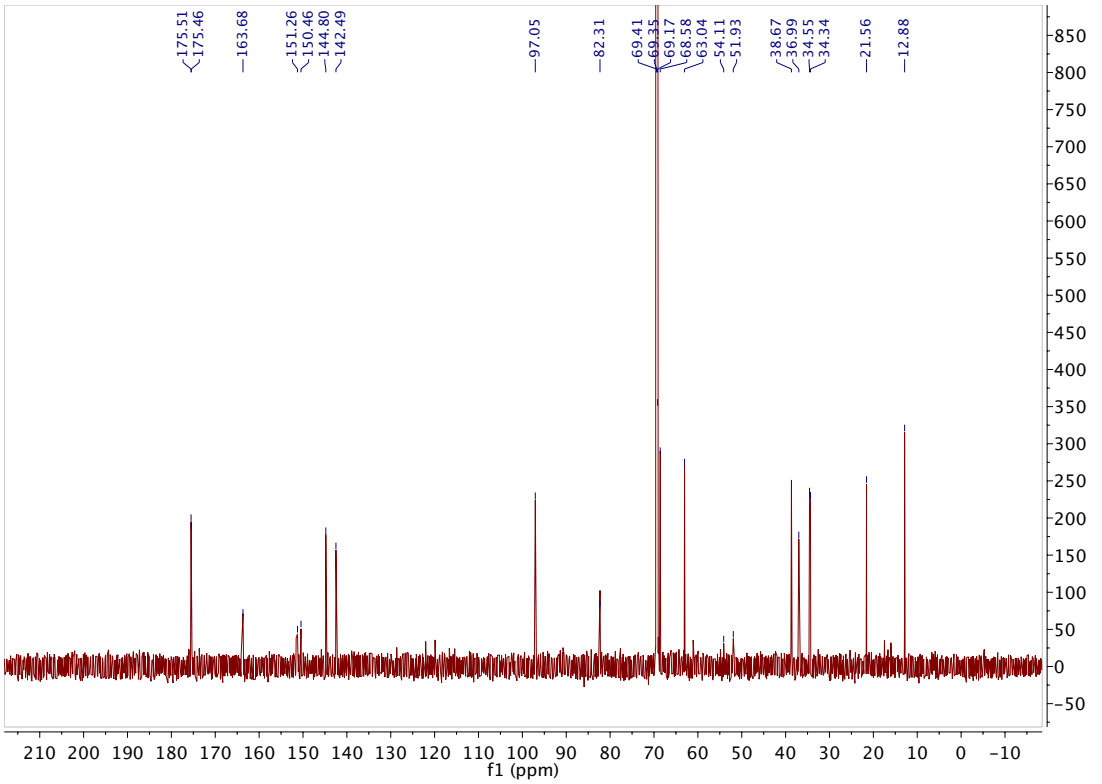
175.51 175.46 163.68 151.26 150.46 144.80 142.49 97.05 82.31 69.41 69.35 69.17 68.58 63.04 54.11 51.93 38.67 36.99 34.55 34.34 21.56 12.88
f1 (ppm)

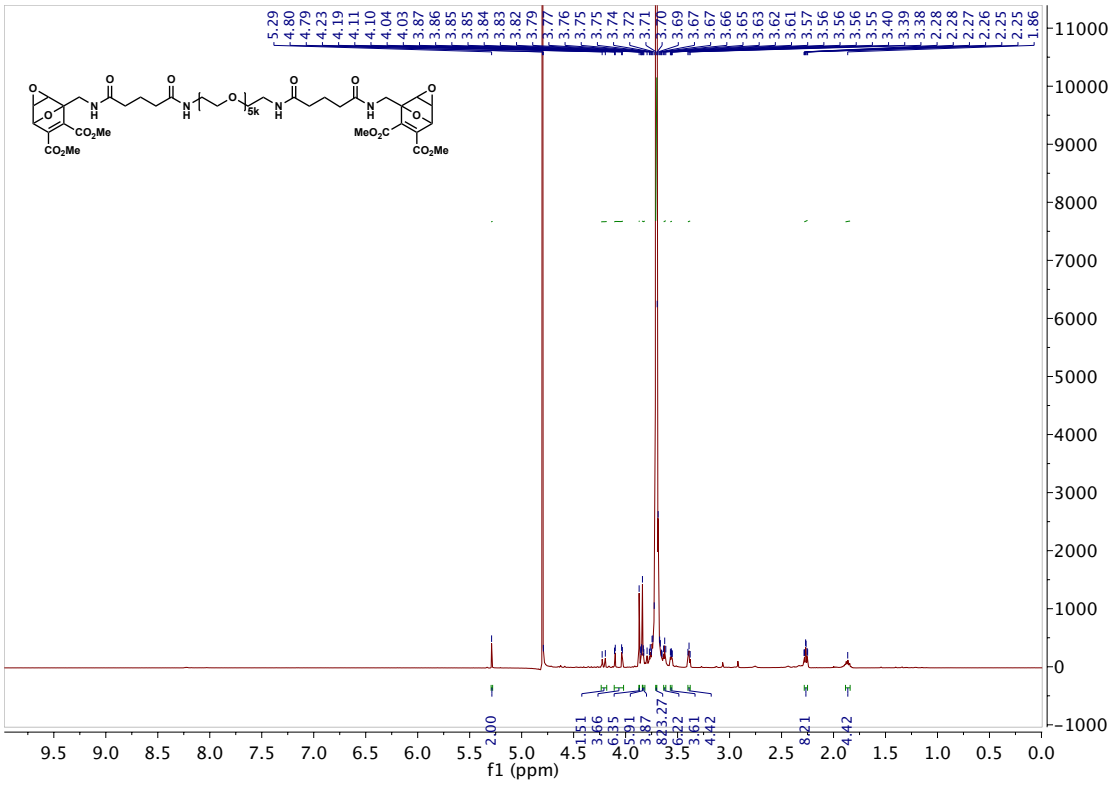
f1 (ppm)

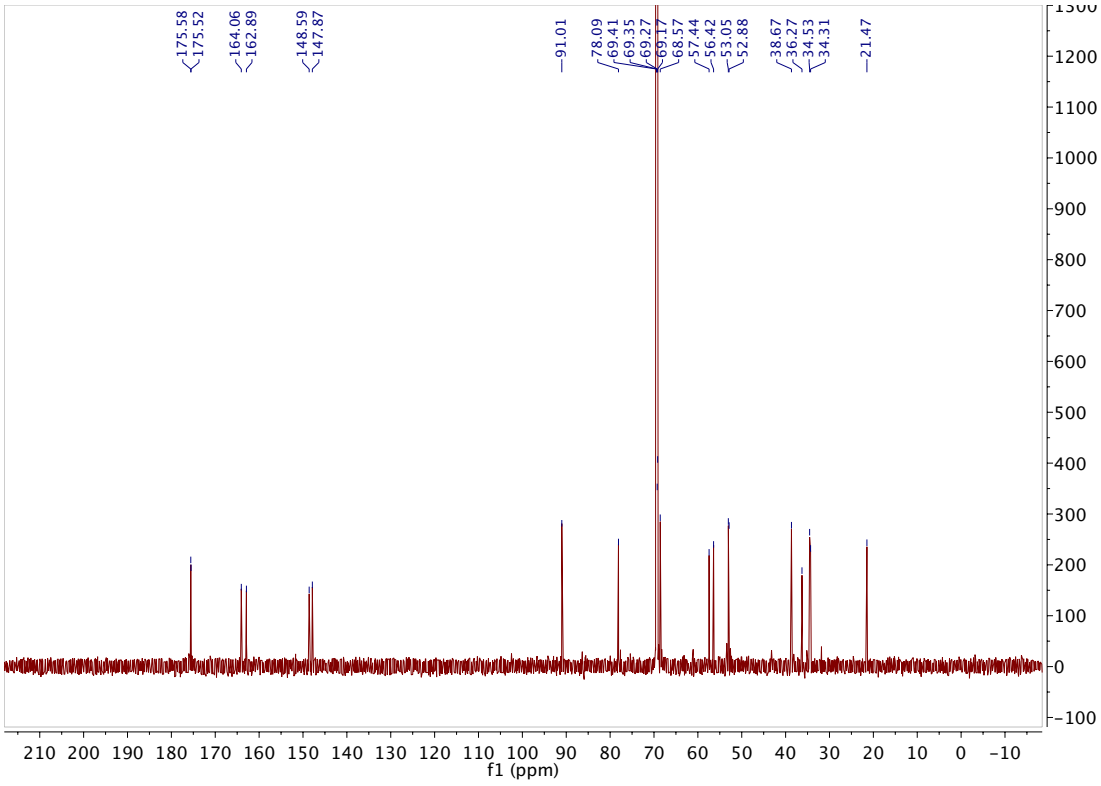
f1 (ppm)

CHAPTER 3. Application of OND Hydrogels in the Treatment of Chronic Wounds

The data presented in this chapter was obtained in experiments carried out by Margarete Daisy Johnson in Dr. Wendy L. Havran's lab at The Scripps Research Institute. All fluorescence images and graphs were provided by Daisy Johnson.

3.1 Introduction

The tunability of oxanorbornadiene hydrogels has been well explored. Simple changes to the OND substitution or crosslinking system yield hydrogels with predictable degradation rates, between hours or months, making them suitable for many therapeutic applications. Here we demonstrate their use in the treatment of chronic wounds.

Chronic wounds affect over 5 million people annually with a significant portion being the elderly population.[32] There are a multitude of different factors that lead to non-healing wounds including cellular changes associated with aging.[33,34] Studies from Dr. Havran's lab have shown that γδ T cells play an important role in wound reepithelialization but are unresponsive and thus unable to promote wound healing in patients with chronic wounds.[35] The binding of junction adhesion molecule like protein (JAML) to coxsackie and adenovirus receptor (CAR) provides costimulation to dendritic epidermal T cells leading to cellular proliferation and cytokine growth. Inhibition of JAML-CAR binding has been shown to lead to decreased dendritic epidermal T cell activation and significant delays in wound healing, similar to what was observed in the absence of γδ T cells.[36] Thus, the binding of JAML to CAR could possibly increase the effectiveness of γδ T cells in chronic wounds to improve wound healing.

Another protein of interest for the treatment of wounds is intercellular adhesion molecule-1 (ICAM-1). ICAM-1 plays an important role in the inflammatory response and it has been shown that lack of expression of the protein leads to significant delays in wound healing, which is commonly seen in aged patients.[37]

The controlled local release of these immune modulating agents directly into wound beds is of important interest for the treatment of chronic wounds. OND hydrogels have been shown to have highly tunable and programable release properties making them suitable for topical wound healing applications. The OND hydrogel delivery of CAR-Fc to CAR null mice as well as the delivery of ICAM-1-Fc to ICAM-1 null and aged mice were investigated and the resulting effects on wound healing are reported.

3.2 Results

3.2.1 Selection of hydrogel material

In order to model the timeline of CAR expression and subsequent dendritic epidermal T cell stimulation seen with normal wound healing, hydrogels should preferentially be able to release all cargo within 24 hours so the entrained protein can reach surrounding wound tissue in a timely manner.[36] Due to their short release timelines methyl ester OND hydrogels **2B** (OND-dextran and divalent PEG-SH, 30 hours) and **2D** (OND-PEG and dextran-SH, 12 hours) were selected for further investigation. In order to validate the release timeline of selected OND hydrogels *in vivo*, reduced Texas Red labeled BSA was encapsulated within hydrogels, the hydrogels were applied to 2 mm wounds on mice, and release of the labeled BSA into surrounding tissue was monitored by fluorescence at different timepoints. BSA was chosen as a model cargo due to its molecular weight, which

is close to that of CAR. The first hydrogel that was investigated was hydrogel **2B** (10 wt%) and the results can be seen in Figure 15. At 24 hours the hydrogels were able to retain dye labeled BSA much better when compared to BSA that was delivered just in buffer, however the hydrogels were not yet fully degraded. At 37 hours the hydrogels were fully degraded and BSA could be seen entering surrounding tissue, however this would miss the therapeutic window for delivery of CAR. In an effort to shorten the release timeline, the same hydrogel system was repeated with 3 wt% gels rather than 10 wt%. However, there were no dramatic differences in fluorescence images when compared to the 10 wt% release experiment seen in Figure 15. Consequently, crosslinking system **2B** was abandoned for this particular application in favor of crosslinking system **2D**, which had the shortest release timeline seen in previously mentioned release studies. At 5 and 8 hours hydrogel **2D** was still intact and was able to retain the BSA Cargo within the wound bed much better than BSA that was delivered in buffer (Figure 16). At 16 hours the gels were almost fully degraded, and dye labeled BSA was beginning to enter surrounding tissue. By 24 hours the gels were fully degraded and BSA-TxRed was no longer in the wound bed. The *in vivo* release timeline of hydrogel **2D** was short enough for entrained cargo to reach surrounding wound tissue in a timely manner and was thus selected for future OND hydrogel delivery to model chronic wounds. In addition, cell viability studies showed that hydrogel 2D was non-toxic to surrounding cells in the epidermis (2.4.5.2 Figure 23).

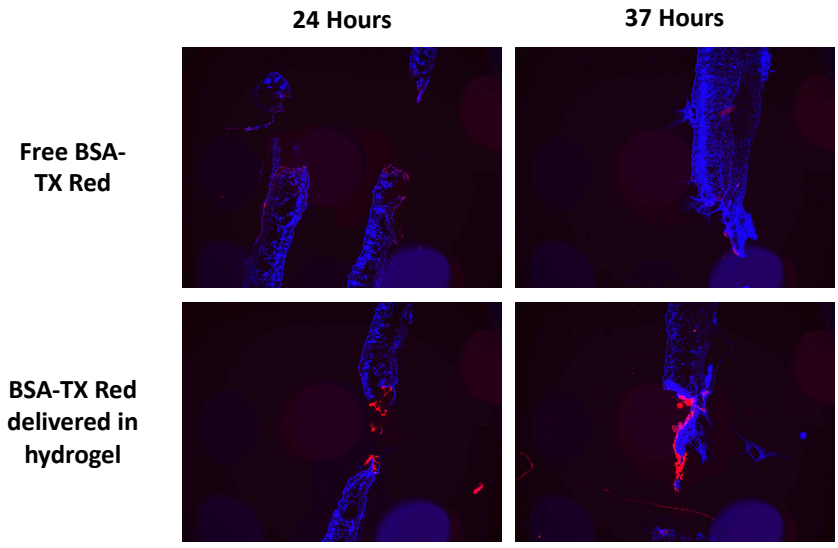

Figure 15. Fluorescent microscopy images of mouse wound beds collected at different times. Mice were given either BSA-TxRed in hydrogel **2B** or in buffer. The blue color is DAPI stain and the red color is BSA-TxRed.

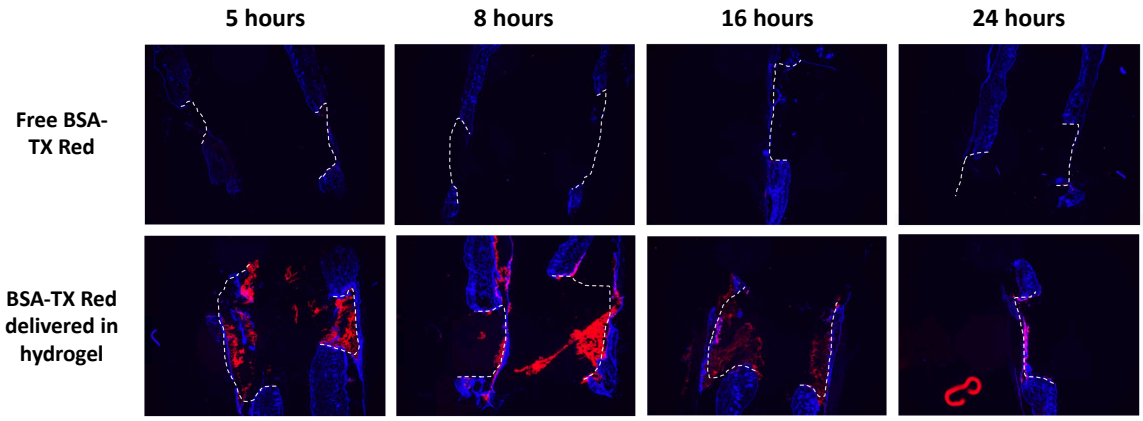

Figure 16. Fluorescent microscopy images of mouse wound beds collected at different times. Mice were given either BSA-TxRed in hydrogel **2D** or in buffer. White dashed lines are outlines of the wound bed, the blue color is DAPI stain, and the red color is BSA-TxRed.

3.2.2 Delivery of CAR-Fc

Delivery of Texas Red labeled CAR from hydrogel **2D** to mice wounds was monitored by fluorescence and compared to results from the BSA-TxRed release studies. In order to conserve material, CAR-Fc was not reduced due to the belief that a free thiol might already be present, and that the protein is large enough to be entrained within the hydrogel network. Fluorescence images collected at 5 and 24 hours showed very similar results when compared to the BSA release study where the labeled CAR delivered in the OND hydrogel was completely retained within the wound bed at 5 hours and had much better retention when compared to labeled CAR delivered in buffer (Figure 17). At 24 hours the hydrogels were completely degraded, labeled CAR was no longer in the wound bed and instead could be detected in surrounding tissue. Since the release timeline of unreduced CAR-Fc matched the release profile of reduced BSA, release studies with CAR-Fc were carried out with unreduced protein.

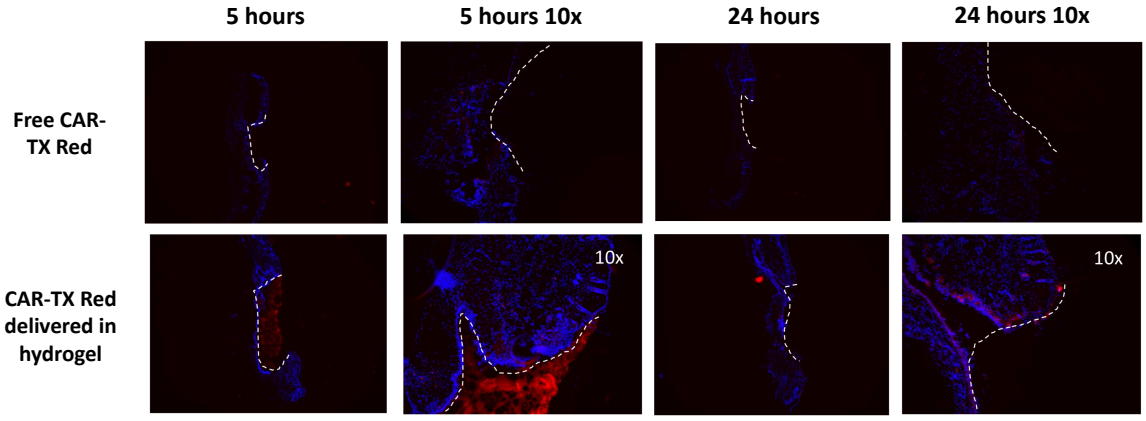

Figure 17. Fluorescent microscopy images of mouse wound beds collected at different times. Mice were given either CAR-TxRed in hydrogel 2D or in buffer. White dashed lines are outlines of the wound bed, the blue color is DAPI stain, and the red color is CAR-TxRed.

In order to assess the effectiveness of CAR-Fc delivery from OND hydrogels to chronic wounds, hydrogels were applied to CAR null mice and the rate of wound closure was monitored. Results of hydrogel delivery of CAR-Fc to CAR null mice were compared against the following groups: wildtype mice that were treated with empty hydrogels (no CAR-Fc) and knockout mice that were treated with buffer. As seen in Figure 18 the effectiveness of OND hydrogel delivery of CAR-Fc to treat model chronic wounds is not initially clear due to the poor separation between wildtype and knockout mice that were treated with buffer. This poor separation is a result of different healing kinetics in the wildtype mice than what is normally seen, which is most likely caused by the bandages that are wrapped around the mice to prevent them from attempting to remove the hydrogels. Since the bandages are essential to maintaining the integrity of the hydrogel throughout wound healing experiments, other wounding strategies were investigated to improve the baseline separation between the knockout and wildtype mice. Increasing the size of the wounds from 2 mm to 3 mm had little effect on the separation between wildtype and knockout mice, however, decreasing the age of the mice from 12 weeks to 8 weeks provided improved separation in wound healing. The OND hydrogel delivery of CAR-Fc to CAR null mice was repeated with 8 week old mice. In addition, a 4th group of mice were added to the experiment in order to observe the effects of CAR-Fc applied in solution to CAR-/- wounds. There was a modest improvement in separation between knockout and wildtype mice, however, CAR-Fc delivered from hydrogels to CAR-/- mice did not improve wound healing rates (Figure 19). Although interestingly, CAR-Fc that was delivered in solution to CAR-/- mice did improve wound healing to rates similar to

wildtype mice. This suggests that CAR-Fc is upregulated very early on after wounding and that extended and controlled delivery of the costimulatory molecule is not beneficial.

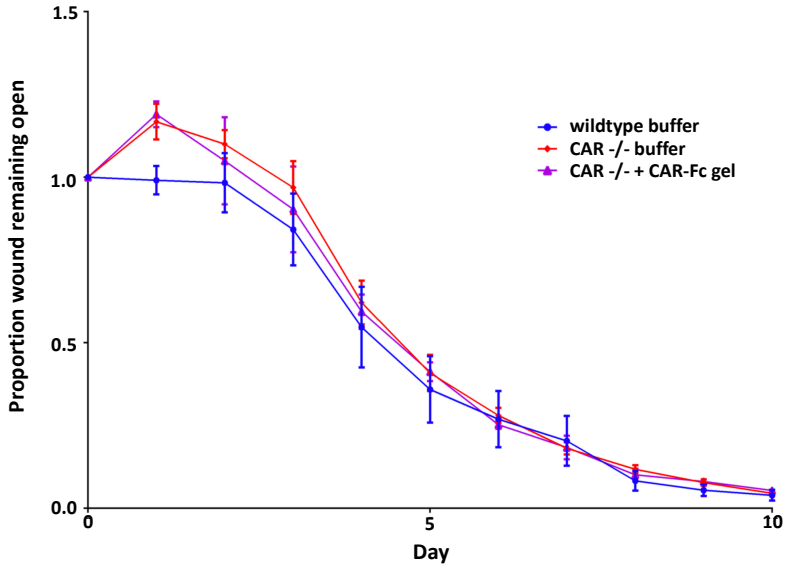

Figure 18. Wound closure in CAR-/- mice treated with CAR-Fc from OND hydrogel 2D. Untreated wildtype and CAR-/- mice were used as controls.

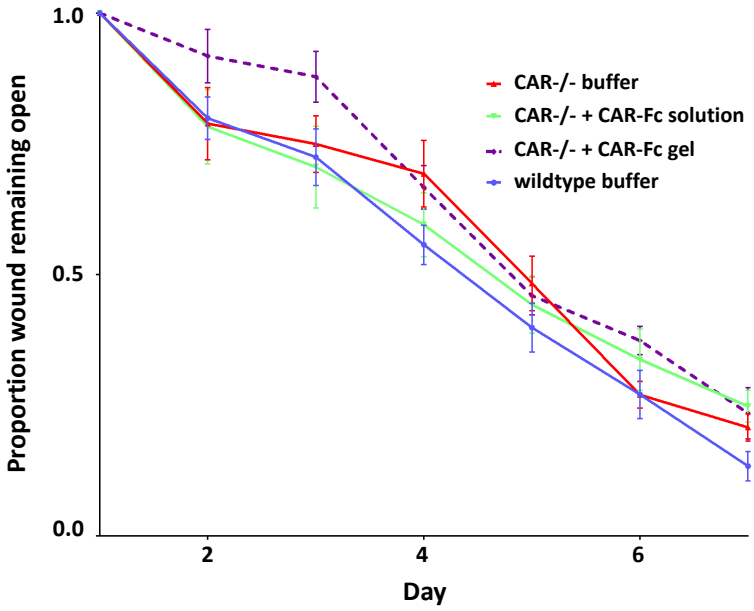

Figure 19. Wound closure in CAR-/- mice treated with CAR-Fc from OND hydrogel 2D or CAR-Fc from solution. Untreated wildtype and CAR-/- mice were used as controls.

3.2.3 Delivery of ICAM-1-Fc

Although controlled and extended delivery of CAR-Fc was not able to improve wound healing in CAR-/- mice, another protein of interest, ICAM-1, was found to promote wound healing under our controlled delivery conditions. The release timeline of ICAM-1-Fc from OND hydrogel **2D** was expected to be similar to the BSA and CAR release studies. However, to confirm that ICAM-1could still be retained in OND hydrogels the protein was labeled with Alexa Fluor 488 and its retention was monitored by fluorescent microscopy. At 5 hours ICAM-1 that was delivered in hydrogels could still be detected within the wound bed whereas ICAM-1 delivered in solution could no longer be seen in or near the wound bed (Figure 20). These results agreed with previous retention and release studies done with

both BSA and CAR-Fc. Consequently, further experiments were carried out with the same OND hydrogel delivery system as the previous experiments.

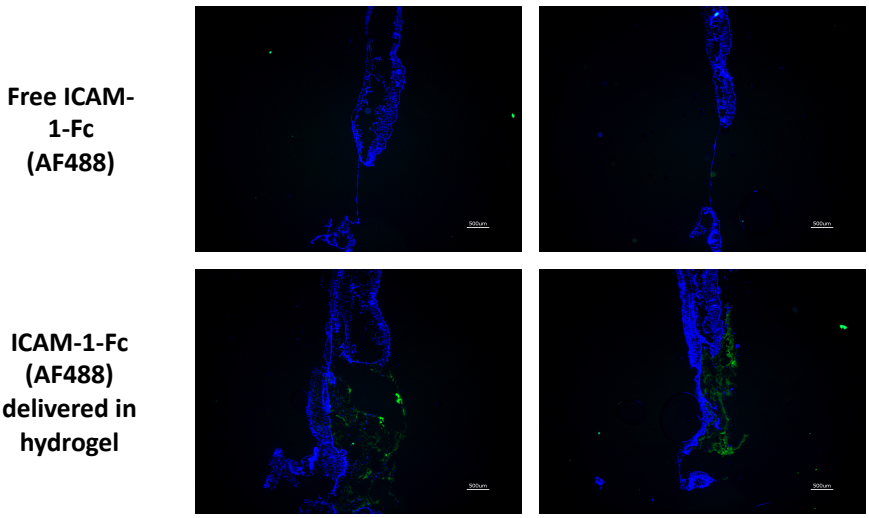

Figure 20. Fluorescent microscopy images of mouse wound beds collected at different times. Mice were given either AF488 labeled ICAM-1-Fc in hydrogel **2D** or in buffer. The blue color is DAPI stain and the green color is AF488 labeled ICAM-1-Fc.

To assess the effectiveness of ICAM-1-Fc delivery from OND hydrogels to wounds, hydrogels were applied to ICAM-1 null mice and the rate of wound closure was monitored. Results of hydrogel delivery of ICAM-1-Fc to ICAM-1 knockout mice were compared against the following three groups: wildtype mice that were treated with empty hydrogels, knockout mice that were treated with buffer, and knockout mice that were treated with ICAM-1-Fc in solution. Knockout mice that were treated with just buffer showed delays in wound healing when compared to wildtype mice. Unlike the CAR-Fc study, delivery of ICAM-1-Fc in solution to ICAM-1 knockout mice showed no

improvement in wound healing when compared to knockout mice with just buffer. Finally, OND hydrogel delivery of ICAM-1-Fc to ICAM-1 knockout mice successfully improved wound healing to rates seen with wildtype mice (Figure 21).

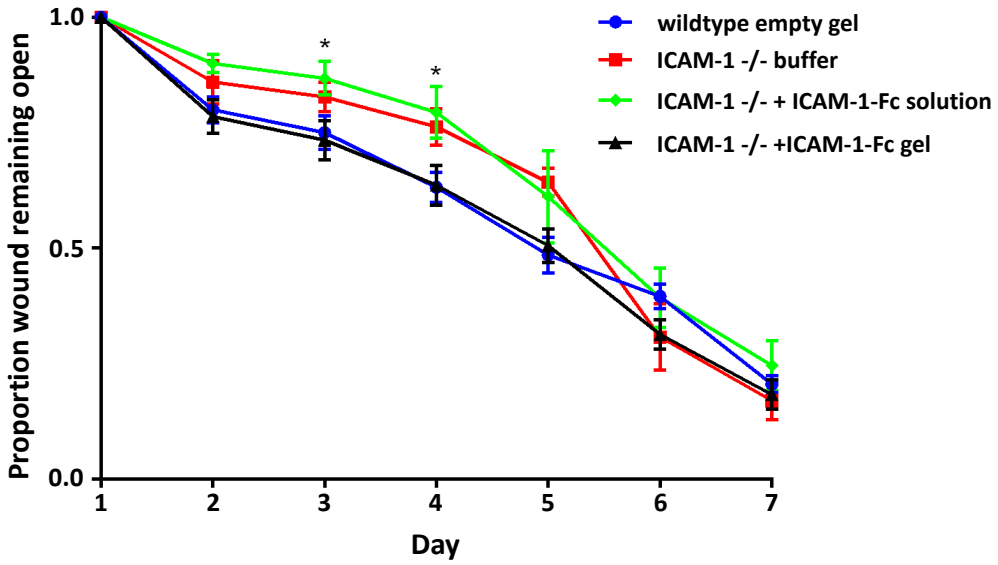

Figure 21. Wound closure in ICAM-1-/- mice treated with ICAM-1-Fc from OND hydrogel 2D or ICAM-1-Fc from solution. Untreated wildtype and ICAM-1-/- mice were used as controls.

We were interested in applying our OND hydrogels to further clinical applications and looked towards aged mice, which often have delayed healing due to dysregulated expression of ICAM-1 following wounding.[37] OND-hydrogels **2D** with either ICAM-1-Fc or buffer were applied to aged mice and the rate of wound closure was monitored. Mice treated with ICAM-1 from OND-hydrogels showed faster wound healing when compared to mice that were given the control gel. This difference in wound healing is especially

apparent by days 5 and 6 (Figure 22). Collectively, controlled and extended delivery of ICAM-1-Fc from OND hydrogels was able to improve wound healing rates in aged mice models.

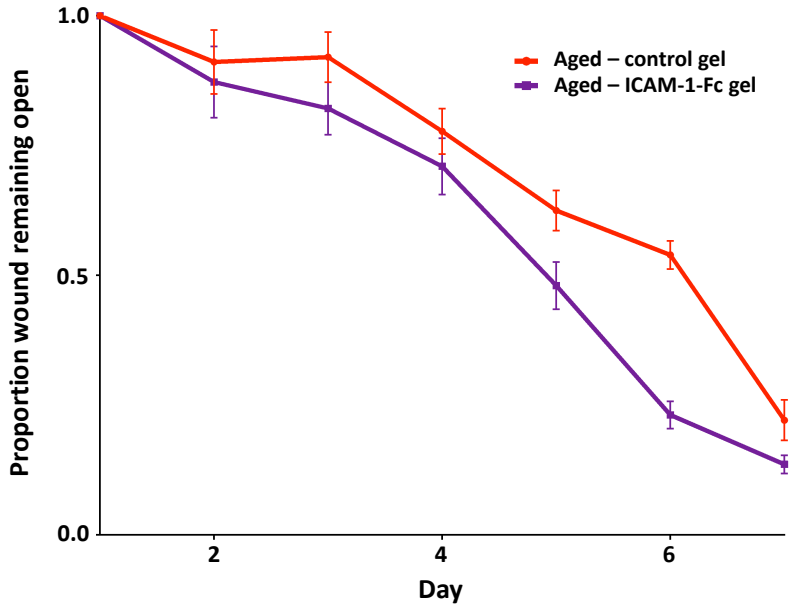

Figure 22. Wound closure in aged mice treated with ICAM-1-Fc from OND hydrogel 2D. Aged mice treated with empty hydrogels (no ICAM-1-Fc) were used as controls.

2.3 Conclusions

Oxanorbornadiene hydrogels were successfully applied to in vivo models seeking to improve chronic wound healing rates. Hydrogel materials were able to retain dye labeled BSA within wound beds and release all cargo at the expected, programmed rates. In addition, hydrogel materials **2D** were found to be non-toxic to surrounding cells (2.4.5.2 Figure 23).

While OND hydrogels were able to deliver CAR-Fc to CAR null mice in the programmed timeframe, it was found that extended delivery of CAR was not beneficial to wound healing in this model as the costimulatory molecule was upregulated very quickly after wounding. Although controlled delivery of CAR was not beneficial, OND hydrogel delivery of ICAM-1-Fc to ICAM-1 null mice was successfully able to improve wound healing rates. These results were reproduced in an aged mice model, showing that delivery of ICAM-1-Fc to aged mice could improve wound healing, which is significant since much of the chronic wound population is elderly. Collectively, the utility of OND hydrogels was demonstrated in *in vivo* models. It is expected that OND hydrogels could be just as useful in applications that require longer delivery timeframes.

2.4 Experimental

2.4.1 In vivo wounding strategies

Isoflurane was administered to mice with a precision vaporizer and a regulated oxygen flow. The incision site was shaved and cleaned with topical disinfectant. Excision wounds were then made on the backs of mice (2-6 wounds/mouse) with a 2 mm biopsy instrument. Gels or PBS (control) were then applied directly to the wound beds and then were covered with bandages.

2.4.2 In vivo delivery of Texas Red labeled BSA

2.4.2.1 Texas Red labeling of bovine serum albumin

1 mL of BSA (5 mg/ml) was incubated with NHS-Texas Red (122.8 μg, 2 equiv.) overnight at room temperature. BSA was separated from excess dye by a PD-10 desalting

column gravity protocol published by the manufacturer. BSA-TxRed was concentrated to 1 mL by centrifugation in 10 kDa MWCO for 8 minutes at 4000x g followed by buffer exchange with 0.001 M potassium phosphate buffer. Protein concentration was measured by Bradford assay with BSA calibration standards. To obtain BSA-TxRed with a free thiol the sample was diluted to 2 mg/mL and treated with 10 mM DTT at 37°C for 1 hour. BSA-TxRed was then purified by PD-10 desalting column with the gravity protocol published by the manufacturer. The sample was concentrated to 1 mL by centrifugation in 10 kDa MWCO for 8 minutes at 4000x g and protein concentration was measured by Bradford assay with BSA calibration standards.

2.4.2.2 Delivery of Texas Red labeled BSA

10 μg BSA-TxRed was delivered in either hydrogel or in PBS directly on mouse wound beds. To make the hydrogels, OND material and thiol material were dissolved separately in 2 mg/mL BSA-TxRed solution in 0.001 M potassium phosphate buffer. The vials were placed on ice and then combined, mixed, and transferred directly to mouse wound beds. For each delivery method (hydrogel or buffer) there were at least two time points with 5 mice each with each mouse having at least 2 wounds. At selected timepoints the mice were sacrificed, and entire wounds were excised, stained with DAPI, and viewed by fluorescence microscopy to detect retention of BSA-TxRed in the wound bed. Delivery of Texas Red labeled BSA was used to screen various OND hydrogels to determine which gel system to use for further delivery studies. It was found that 10 wt% OND-PEG gels had the fastest release and thus were chosen for further experiments.

2.4.3 In vivo delivery of CAR-Fc from OND hydrogels

10 μg CAR-Fc was delivered to either CAR knockout mice or wildtype mice in either hydrogel or potassium phosphate buffer. To make the hydrogels, PEG-OND material and dextran-thiol material were dissolved separately in CAR-Fc solution in 0.001 M potassium phosphate buffer. The vials were placed on ice and then combined, mixed, and transferred directly to mouse wound beds. Effects of hydrogel delivery of CAR-Fc to CAR knockout mice were compared against the following three groups: wildtype mice that were treated with empty hydrogels (no CAR-Fc), knockout mice that were treated with buffer, and knockout mice that were treated with CAR-Fc in solution. Each group had 3 mice with 2 wounds per mouse for each timepoint. Wound healing was assessed by rate of wound closure.

2.4.4 In vivo delivery of ICAM-1-Fc from OND hydrogels

10 μg ICAM-1-Fc was delivered to either I-CAM-1 knockout mice or wildtype mice in either hydrogel or potassium phosphate buffer. To make the hydrogels, PEG-OND material and dextran-thiol material were dissolved separately in ICAM-1-Fc solution in 0.001 M potassium phosphate buffer. The vials were placed on ice and then combined, mixed, and transferred directly to mouse wound beds. Effects of hydrogel delivery of ICAM-1-Fc to ICAM-1 knockout mice were compared against the following three groups: wildtype mice that were treated with empty hydrogels (no ICAM-1-Fc), knockout mice that were treated with buffer, and knockout mice that were treated with ICAM-1-Fc in solution. Each group had 3 mice with 2 wound per mouse for each timepoint. Wound healing was measured by the undermentioned assays.

2.4.5 Wound healing assays

2.4.5.1 Determination of the rate of wound closure

For each timepoint, wounds were photographed and the diameter of at least 3 wounds were measured three times. Statistical significance was determined by an unpaired 2-tailed Student t-test.

2.4.5.2 Analysis of cell viability post hydrogel treatment

Toxicity of hydrogel materials were assessed by 7-Aminoactinomycin D viability stain and flow cytometry of dendritic epidermal T cells 24 hours following wounding. Percent apoptotic cells were determined by Annexin-V staining in epidermal sheets following wounding. 5 μL of either hydrogel material or PBS were delivered directly on mouse wound beds. There were 4 mice in each group with each mouse having four wounds.

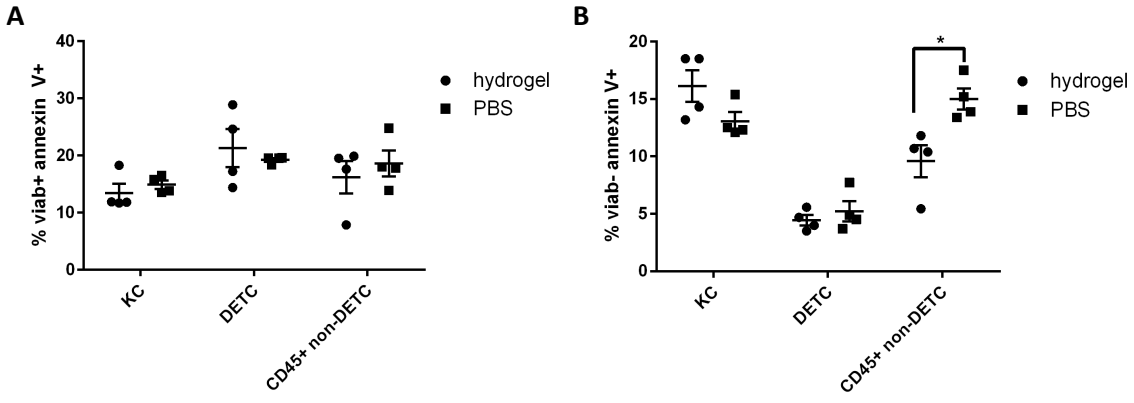

Figure 23. Cell viability post hydrogel 2D treatment. (A) dead cells. (B) dying cells.

CHAPTER 4. Conclusions and Future Directions

Hydrogel delivery systems have greatly improved over the past few decades and are now able to achieve controlled and sustained delivery of therapeutics over longer timeframes. However, many of these delivery systems are not easily tunable to achieve different release profiles, which limits their potential applications. Thus, materials that are able to be broadly useful for a variety of applications from drug delivery to tissue engineering remain an unmet need in the field of hydrogel systems. Oxanorbornadiene reagents have been shown to have highly tunable fragmentation rates from hours to months, making them promising as cleavable linkages in degradable hydrogels. This thesis furthers the scope of oxanorbornadiene hydrogels in therapeutic applications.

In chapter 2 the effects of different crosslinking compositions on hydrogel properties was explored. In total, 12 different hydrogels were synthesized with 3 different ONDs and 4 different crosslinking systems. All hydrogels were fully formed in less than 20 seconds at physiological pH and had high material incorporation and low swelling ratios. It was found that methyl ester OND hydrogels could be tuned to deliver entrained cargo over 12 to 66 hours depending on the crosslinking system. As expected, trifluoromethyl ONDs had much longer release timelines and were able to deliver entrained cargo over 7 to 25 days depending on the crosslinking system. Epoxide gels were non-degradable and were unable to release entrained cargo, which demonstrated the dependence of cargo release on the retro-Diels-Alder reactions of OND linkages.

Chapter 3 examined the translation of OND hydrogels to *in vivo* experiments seeking to promote improved healing in chronic wounds. Hydrogels were easily applied to wound beds by separately dissolving OND and thiol material, combining solutions, and depositing the hydrogel solution directly onto wounds. Hydrogel materials were found to be non-toxic and were able to release cargo into surrounding wound tissue within the programmed timeframes. Delivery of CAR-Fc to CAR null mice was able to improve wound healing, however, these improvements were not achieved by hydrogel delivery, suggesting that extended delivery of the costimulatory molecule is not necessary. In contrast, OND hydrogel delivery of ICAM-1-Fc to ICAM-1 null mice was necessary in order to successfully improve wound healing rates to what was observed with wildtype mice. Lastly, OND hydrogel delivery of ICAM-1-Fc was able to improve wound healing rates in aged mice, which is significant since much of the chronic wound population is elderly.

In the future, we hope to expand the utility of OND hydrogels by investigating them in the context of different delivery methods and applications. The implementation of OND hydrogels for topical delivery has been demonstrated in this work. We are next interested in developing OND hydrogels as injectable depots. There are many advantages to injectable depot drug delivery systems including their ability to localize therapeutics, reduce off-target effects, and be applied directly to tissues of interest without surgical implantation. We believe that OND hydrogels will be amenable to this delivery system due to their rapid gelation at physiological pH and temperature. Continuing to investigate OND hydrogels will further the goal of realizing simple hydrogel drug delivery systems that can be broadly useful to applications requiring controlled release over hours or months.

REFERENCES

1. Fenton, Owen S., Katy N. Olafson, Padmini S. Pillai, Michael J. Mitchell, and Robert Langer. "Advances in Biomaterials for Drug Delivery." *Advanced Materials* 30.29 (2018): 1705328.

2. Tibbitt, Mark W., James E. Dahlman, and Robert Langer. "Emerging Frontiers in Drug Delivery." *Journal of the American Chemical Society* 138.3 (2016): 704-17.

3. Kharkar, Prathamesh M., Kristi L. Kiick, and April M. Kloxin. "Designing Degradable Hydrogels for Orthogonal Control of Cell Microenvironments." *Chem. Soc. Rev.* 42.17 (2013): 7335-372.

4. Li, Jianyu, and David J. Mooney. "Designing Hydrogels for Controlled Drug Delivery." *Nature Reviews Materials* 1.12 (2016): n. pag.

5. Momoh, Frederick U., Joshua S. Boateng, Simon C.w. Richardson, Babur Z. Chowdhry, and John C. Mitchell. "Development and Functional Characterization of Alginate Dressing as Potential Protein Delivery System for Wound Healing." *International Journal of Biological Macromolecules* 81 (2015): 137-50.

6. Wichterle, O., and D. Lím. "Hydrophilic Gels for Biological Use." *Nature* 185.4706 (1960): 117-18.

7. R.M. Nalbandian, R.L. Henry, H.S. Wilks, Artificial skin. II. Pluronic F-127 Silver nitrate or silver lactate gel in the treatment of thermal burns, J. Biomed. Mater. Res. 6 (1972) 583–590.

8. Jeon, Oju, Caitlin Powell, Loran D. Solorio, Melissa D. Krebs, and Eben Alsberg. "Affinity-based Growth Factor Delivery Using Biodegradable, Photocrosslinked Heparin-alginate Hydrogels." *Journal of Controlled Release* 154.3 (2011): 258-66.

9. Ogle, Molly E., Jack R. Krieger, Liane E. Tellier, Jennifer Mcfaline-Figueroa, Johnna S. Temenoff, and Edward A. Botchwey. "Dual Affinity Heparin-Based Hydrogels Achieve Pro-Regenerative Immunomodulation and Microvascular Remodeling." *ACS Biomaterials Science & Engineering* 4.4 (2017): 1241-250.

10. Li, Jun, Xu Li, Xiping Ni, Xin Wang, Hongzhe Li, and Kam W. Leong. "Self-assembled Supramolecular Hydrogels Formed by Biodegradable PEO–PHB–PEO Triblock Copolymers and α-cyclodextrin for Controlled Drug Delivery." *Biomaterials* 27.22 (2006): 4132-140.

11. Li, Jun, Xiping Ni, and Kam W. Leong. "Injectable Drug-delivery Systems Based on Supramolecular Hydrogels Formed by Poly(ethylene Oxide)s and ?-cyclodextrin." *Journal of Biomedical Materials Research* 65A.2 (2003): 196-202.

12. Mealy, Joshua E., Christopher B. Rodell, and Jason A. Burdick. "Sustained Small Molecule Delivery from Injectable Hyaluronic Acid Hydrogels through Host–guest Mediated Retention." *Journal of Materials Chemistry B* 3.40 (2015): 8010-019.

13. Ashley, G. W., J. Henise, R. Reid, and D. V. Santi. "Hydrogel Drug Delivery System with Predictable and Tunable Drug Release and Degradation Rates." *Proceedings of the National Academy of Sciences* 110.6 (2013): 2318-323.

14. Kloxin, April M., Andrea M. Kasko, Chelsea N. Salinas, and Kristi S. Anseth. "Photodegradable Hydrogels for Dynamic Tuning of Physical and Chemical Properties." *Science* 324.5923 (2009): 59-63.

15. Griffin, Donald R., and Andrea M. Kasko. "Photodegradable Macromers and Hydrogels for Live Cell Encapsulation and Release." *Journal of the American Chemical Society* 134.31 (2012): 13103-3107.

16. Yan, Bin, John-Christopher Boyer, Damien Habault, Neil R. Branda, and Yue Zhao. "Near Infrared Light Triggered Release of Biomacromolecules from Hydrogels Loaded with Upconversion Nanoparticles." *Journal of the American Chemical Society* 134.40 (2012): 16558-6561.

17. Martens, Penny J., Stephanie J. Bryant, and Kristi S. Anseth. "Tailoring the Degradation of Hydrogels Formed from Multivinyl Poly(ethylene Glycol) and Poly(vinyl Alcohol) Macromers for Cartilage Tissue Engineering." *Biomacromolecules* 4.2 (2003): 283-92.

18. Hiemstra, Christine, Zhiyuan Zhong, Sophie R. Van Tomme, Mies J. Van Steenbergen, John J.l. Jacobs, Willem Den Otter, Wim E. Hennink, and Jan Feijen. "In Vitro and in Vivo Protein Delivery from in Situ Forming Poly(ethylene Glycol)–poly(lactide) Hydrogels." *Journal of Controlled Release* 119.3 (2007): 320-27.

19. Xu, Qian, Linru Guo, Sigen A, Yongsheng Gao, Dezhong Zhou, Udo Greiser, Jack Creagh-Flynn, Hong Zhang, Yixiao Dong, Lara Cutlar, Fagang Wang, Wenguang Liu, Wei Wang, and Wenxin Wang. "Injectable Hyperbranched Poly(β-amino Ester) Hydrogels with On-demand Degradation Profiles to Match Wound Healing Processes." *Chemical Science* 9.8 (2018): 2179-187.

20. Lévesque, Stéphane G., and Molly S. Shoichet. "Synthesis of Enzyme-Degradable, Peptide-Cross-Linked Dextran Hydrogels." *Bioconjugate Chemistry* 18.3 (2007): 874-85.

21. Oommen, Oommen P., Shujiang Wang, Marta Kisiel, Marije Sloff, Jöns Hilborn, and Oommen P. Varghese. "Smart Design of Stable Extracellular Matrix Mimetic Hydrogel: Synthesis, Characterization, and In Vitro and In Vivo Evaluation for Tissue Engineering." *Advanced Functional Materials* 23.10 (2012): 1273-280.

22. Peppas, N. A., J. Z. Hilt, A. Khademhosseini, and R. Langer. "Hydrogels in Biology and Medicine: From Molecular Principles to Bionanotechnology." *Advanced Materials* 18.11 (2006): 1345-360.

23. Hong, Vu, Alexander A. Kislukhin, and M. G. Finn. "Thiol-Selective Fluorogenic Probes for Labeling and Release." *Journal of the American Chemical Society* 131.29 (2009): 9986-994.

24. Kislukhin, Alexander A., Cody J. Higginson, Vu P. Hong, and M. G. Finn. "Degradable Conjugates from Oxanorbornadiene Reagents." *Journal of the American Chemical Society* 134.14 (2012): 6491-497.

25. Fell, Jason S., Steven A. Lopez, Cody J. Higginson, M. G. Finn, and K. N. Houk. "Theoretical Analysis of the Retro-Diels–Alder Reactivity of Oxanorbornadiene Thiol and Amine Adducts." *Organic Letters* 19.17 (2017): 4504-507.

26. Higginson, Cody J., Marsha R. Eno, Susan Khan, Michael D. Cameron, and M.G. Finn. "Albumin-Oxanorbornadiene Conjugates Formed Ex Vivo for the Extended Circulation of Hydrophilic Cargo." *ACS Chemical Biology* 11.8 (2016): 2320-327.

27. Higginson, Cody J., Seung Yeon Kim, Miguel Peláez-Fernández, Alberto Fernández-Nieves, and M.g. Finn. "Modular Degradable Hydrogels Based on Thiol-Reactive Oxanorbornadiene Linkers." *Journal of the American Chemical Society* 137.15 (2015): 4984-987.

28. Mcarthur, Sally L., Keith M. Mclean, Peter Kingshott, Heather A.w. St John, Ronald C. Chatelier, and Hans J. Griesser. "Effect of Polysaccharide Structure on Protein Adsorption." *Colloids and Surfaces B: Biointerfaces* 17.1 (2000): 37-48. Print.

29. Yamaoka, Tetsuji, Yasuhiko Tabata, and Yoshito Ikada. "Comparison of Body Distribution of Poly(vinyl Alcohol) with Other Water-soluble Polymers after Intravenous Administration." *Journal of Pharmacy and Pharmacology* 47.6 (1995): 479-86. Print.

30. Huang, Xiao, and Christopher S. Brazel. "On the Importance and Mechanisms of Burst Release in Matrix-controlled Drug Delivery Systems." *Journal of Controlled Release* 73.2-3 (2001): 121-36.

31. Hiemstra, Christine, Leonardus J. Van Der Aa, Zhiyuan Zhong, Pieter J. Dijkstra, and Jan Feijen. "Rapidly in Situ-Forming Degradable Hydrogels from Dextran Thiols through Michael Addition." *Biomacromolecules* 8.5 (2007): 1548-556.

32. Sen, Chandan K., Gayle M. Gordillo, Sashwati Roy, Robert Kirsner, Lynn Lambert, Thomas K. Hunt, Finn Gottrup, Geoffrey C. Gurtner, and Michael T. Longaker. "Human Skin Wounds: A Major and Snowballing Threat to Public Health and the Economy." *Wound Repair and Regeneration* 17.6 (2009): 763-71.

33. Mustoe, Thomas. "Understanding Chronic Wounds: A Unifying Hypothesis on Their Pathogenesis and Implications for Therapy." *The American Journal of Surgery* 187.5 (2004)

34. Gould, Lisa, Peter Abadir, Harold Brem, Marissa Carter, Teresa Conner-Kerr, Jeff Davidson, Luisa Dipietro, Vincent Falanga, Caroline Fife, Sue Gardner, Elizabeth Grice, John Harmon, William R. Hazzard, Kevin P. High, Pamela Houghton, Nasreen Jacobson, Robert S. Kirsner, Elizabeth J. Kovacs, David Margolis, Frances Mcfarland Horne, May J. Reed, Dennis H. Sullivan, Stephen Thom, Marjana Tomic-Canic, Jeremy Walston, Jo Anne Whitney, John Williams, Susan Zieman, and Kenneth Schmader. "Chronic Wound Repair and Healing in Older Adults: Current Status and Future Research." *Journal of the American Geriatrics Society* 63.3 (2015): 427-38.

35. Jameson, J., Karen Ugarte, Nicole Chen, Pia Yachi, Elaine Fuchs, Richard Boismenu, and Wendy L. Havran. "A Role for Skin Gamma Delta T Cells in Wound Repair." *Science* 296.5568 (2002): 747-49.

36. Witherden, D. A., P. Verdino, S. E. Rieder, O. Garijo, R. E. Mills, L. Teyton, W. H. Fischer, I. A. Wilson, and W. L. Havran. "The Junctional Adhesion Molecule JAML Is a Costimulatory Receptor for Epithelial T Cell Activation." *Science* 329.5996 (2010): 1205-210.

37. Brubaker, Aleah L., Juan L. Rendon, Luis Ramirez, Mashkoor A. Choudhry, and Elizabeth J. Kovacs. "Reduced Neutrophil Chemotaxis and Infiltration Contributes to Delayed Resolution of Cutaneous Wound Infection with Advanced Age." *The Journal of Immunology* 190.4 (2013): 1746-757.